Dalton Transactions

Accepted Manuscript

ROYAL SOCIETY OF CHEMISTRY

www.rsc.org/dalton

Molecular and Electronic Structure of Nonradical Homoleptic Pyridyl-azo-oxime Complexes of Cobalt(III) and the Azo-Oxime Anion Radical Congener: An Experimental and Theoretical Investigation†

Shuvam Pramanik,[a] Sima Roy,[a] Tapas Ghorui,[a] Sanjib Ganguly*[b] and Kausikisankar Pramanik*[a]

[a]*Department of Chemistry, Inorganic Chemistry Section, Jadavpur University, Kolkata – 700032, India. E-mail: kpramanik@hotmail.com, Tel: +9133 2457 2781*

[b]*Department of Chemistry, St. Xavier's College, Kolkata – 700016, India*

Abstract

The reaction between a potential flexidentate pyridyl-azo-oxime HL **1** and $Co(ClO_4)_2$ yields novel homoleptic complexes of types $[Co^{III}(L^{-I})_3]$ **2** and $[Co^{III}(L^{-I})_2]ClO_4$, $\mathbf{3^+ClO_4}$ in N_6 and N_4O_2 coordination environments respectively. The FMOs of these complexes vary appreciably and are strongly modified by the coordination environment. This has striking influences on the spectral and redox properties of the metallo conjugates of ligand HL. The synthesized bis **2** and tris chelates $\mathbf{3^+}$ possess well-defined optoelectronic and redox properties and these are scrutinized by the Density Functional Theory (DFT) and Time Dependent Density Functional Theory (TD-DFT) analysis. The visible excitations are primarily mixed singlet-manifold ^{1}ILCT and ^{1}LLCT transitions, with different amount of ligand π−π* character while in the UV region, the excitations are essentially π−π* ILCT/LLCT transitions for the $\mathbf{3^+}$ and ILCT/LLCT transitions along with LMCT component for **2**. The luminescent cobalt(III) species are rarely cited albeit these are found to be moderately blue emissive with slight quenching of the emission quantum yield (*Φ*) as compared to that of free ligand. Computation reveals that the cobalt *d* orbital is involved in the triplet emissive excited states and this phenomenon is plausibly responsible for the quenching of the emission quantum yield in the complexes. Both types of complexes are electro-active in solution and the first reductive response, associated with the redox orbital comprising delocalized π orbital of ligand, is shifted in the more positive potential (0.6 V *vs*. Ag/AgCl) in $\mathbf{3^+}$ relative to **2** and this observation is corroborated with the appreciable stabilization (~0.5 eV) of LUMO of $\mathbf{3^+}$ (coordination mode **A**) as compared to that in **2** (coordination mode **B**). This provides us an opportunity to explore the cobalt-bound azo-oxime anion radical compound by reduction of the diamagnetic precursor $\mathbf{3^+}$. The best description of the one-electron paramagnetic **3** can be ascertained as $[Co^{III}\{(L^{-I})_2\}^{\bullet-}]$ from the EPR and DFT studies where the unpaired spin is delocalizes essentially over π* orbital comprising both the coordinated ligands (97%) with little participation of cobalt d_{yz} (3%).

Introduction

Cobalt-oxime complexes are of intriguing interest since their documentation by Schrauzer *et al*[1] due to their close resemblance with cobalamins (Vitamin B_{12}). Such compounds comprising of non-precious metal have recently emerged as potential homogeneous catalysts for hydrogen evolution in protic solvent,[2] biocatalysts[3] and a significant number of studies have been performed to understand the underlying chemistry of their electro- and photocatalytic activities.[4] In this context, the use of small and smart donors like pyridine can appreciably alter the catalytic behaviour of cobaloximes by its axial coordination via linking of a functionalized photosensitizer (PS) to the cobalt center.[5]

Notably, the close environment of the metal center in cobaloximes reported so far comprises of conjugated oxime and imine moieties and in some cases pyridine molecule as coligand. It is now of interest to explore the chemistry of cobalt-oxime complexes ligated by organic component incorporating π-acidic moieties like pyridyl, azo and so forth in presence of oxime within the same organic chromophore, since π-acidic chromophores are able to stabilize lower oxidation state of the metal ion or they themselves assume one or more electrons upon coordination.[6] In addition, cobalt compounds incorporating a photosensitizer (PS) oxime chromophore can behave as an electron source for proton reduction as well as a means of electron transfer to the catalyst via absorption of light. In this regard, the study of the molecular and electronic structures of novel cobalt-oxime complexes is vital for the investigation of electron transfer as well as optoelectronic properties within the metal-organic hybrids.

In the present work, we chose a multifunctional and flexidentate oxime ligand **1** incorporating azo and pyridyl groups as basic organic chromophore (Scheme 1). These are rare

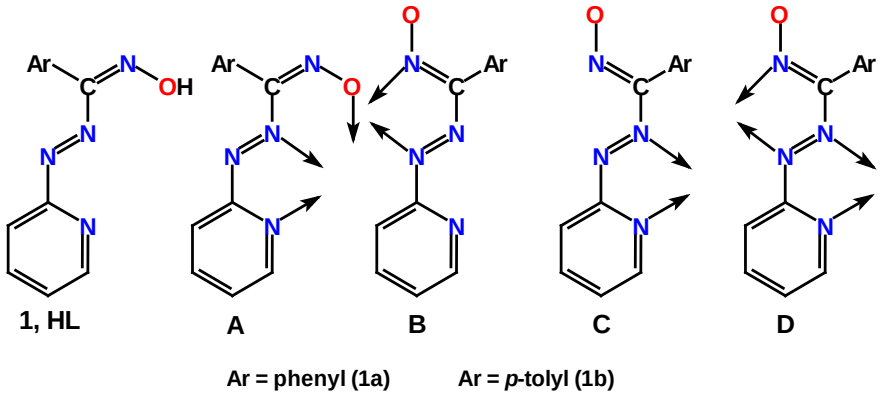

Scheme 1 Aryl-azo-oxime and its different chelation modes

examples of typical nitrogen-rich azo-aromatic molecule possessing low-lying vacant π* molecular orbital delocalized primarily over azo along with substantial contribution of pyridyl and oxime moieties.

These types of ligands are apposite to act as potentially redox non-innocent upon coordination.[7] Some ligands can exist in nature in more than one oxidation states Moreover, the titled ligands have been found to behave as fluorophore and this is another prime reason for their selection. Emissive behaviour of such organic chromophores also prevails in their metallo conjugates with cobalt(III) and such event offers an opportunity to scrutinize luminescence behaviour of cobalt(III) compounds, due to the paucity of analogous studied in the literature.[8] Although a number of chelation modes are apparent with $\mathbf{L}^{-}$ (Scheme 1), the mode of type **A** is found exclusively with M^{II} (M = Mn,[9b] Fe[9b] and Ni[9a]), furnishing bis-chelates. In contrast, we are successfully able to isolate two different forms of cobalt(III) complexes with **1** *viz*. $[Co^{III}(L^{-I})_3]$ **2** and $[Co^{II}(L^{-I})_2]ClO_4$, $\mathbf{3^+ClO_4^-}$ in N_6 and N_4O_2 coordination environments respectively (Scheme 2), indicating the flexible nature of pyridyl-azo-oxime during chelation with transition metals ions. Both the complexes of type **2** and $\mathbf{3^+ClO_4^-}$ have been meticulously characterized by spectroscopic techniques and their structures were authenticated by X-ray diffraction study.

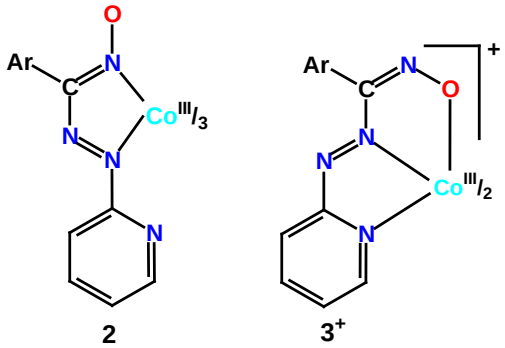

Scheme 2 Different coordination of **1** toward cobalt(III) in bis and tris-chelate complexes

These homoleptic compounds are electro-active in solution and display a series of electron transfer processes. Notably, bis chelates of type $\mathbf{3}^+$ exhibit more facile reduction as compared to the tris chelates **2**. It is worth mentioning that we have been able to isolate the Co(III)-bound anion radical complexes of type **3** in excellent yield in the solid state from their non-radical precursors $\mathbf{3}^+$, where the ligated oximato ligand behaves as electron acceptor. To the best of our knowledge these are the first examples of cobalt (III)-stabilized azo-oxime anion

radical complexes. Finally, unification and correlation of the observed trends in terms of spectral, electrochemical, structure and bonding are scrutinized with the aid of theoretical study.

Results and Discussion

Synthesis

The ligands used in the present work *viz*. HL^{Ph} (**1a**) and HL^{Tol} (**1b**) have been synthesized starting from 2-hydrazinopyridine (Scheme 3). The first step involves synthesis of the hydrazone which is subsequently treated with n-butyl nitrite in presence of sodium ethoxide in ethanol to form sodium salt of the pyridyl azo oximate $Na^{+}L^{-}$. Finally, the aqueous ethanolic solution of $Na^{+}L^{-}$ was neutralized with dilute sulfuric acid and HL was obtained in moderate yield by

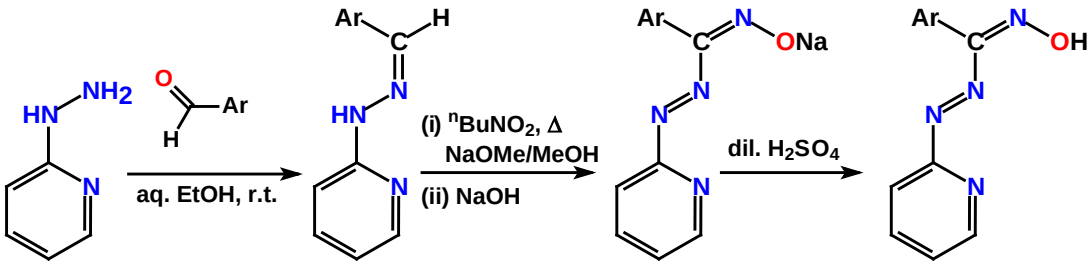

Scheme 3 Ligand synthesis

extracting with dichloromethane. The ligands offer two different types of coordinating N atoms *viz*. pyridyl-N and azo-N that can behave as typical π-acceptor, whereas the oximato-O may behave as π-donor and behave as monoanionic in both the cases. Upon stirring an ethanolic solution of HL, **1,** with $Co(ClO_4)_2{\cdot}6H_2O$ in 2:1 molar ratio, a dark coloured solid was obtained. Recrystallization with dichloromethane-hexane leads to precipitation of the dark brown crystalline bis-chelate of type $[Co^{III}(L^{-I})_2]ClO_4$, $\mathbf{3^{+}ClO_4^{-}}$ in excellent yield while the superincumbent solution remained violet. The violet solution was decanted off and evaporated to dryness to obtain the dark violet crystalline tris-chelate $[Co^{III}(L^{-I})_3]$, **2**, in moderate yield. The yield of **2** can be enhanced appreciably by carrying out the reaction in 1:3 molar ratio of $Co(ClO_4)_2.6H_2O$ and **1**, when $\mathbf{3^{+}ClO_4^{-}}$ is formed in comparatively lower yield. Notably, the chelation mode of type **B** has been found in **2** while in the case of $\mathbf{3^{+}}$ the mode of chelation is of type **A**, indicating the flexidentate nature of pyridyl-azo-oxime for the first time with the same

transition metal for a particular oxidation state. It is worth mentioning that the analogous ligands with comparatively lower π-acidity *viz*. aryl-azo-oximes always behaved as bidentate (chelation mode **B**) in presence of the first transition elements as well as with selected second and third row transition elements.[10] It has been found that for the coordination mode **B**, the donor atoms *viz*. azo-N and oximato-N are disposed in meridional fashion with Co(III) and validates exclusively mononuclear complexes in the present work while the facial disposition of three oximato-O atoms for this coordination mode of HL render the possibility of polynucleation.[11,12] In the bis and tris chelate complexes, the titled ligand coordinated as uninegative tridentate and uninegative bidentate respectively. Moreover, unlike **2** (coordinating environment N_6), N_4O_2 coordinated $\mathbf{3}^+$ (S = 0) species are more prone to reduction and eventually we are able to isolate the neutral complexes of type **3** (S = ½) as stable anion radical in excellent yield by both chemical and electrochemical reduction methods. It is worth mentioning that $\mathbf{3}^+$ represents an uncommon example where the coordinating environment (chelation mode **A** *vs.* **B**) makes the titled oxime ligand more accessible to assume an unpaired spin.

Crystal Structure

The homoleptic tris (**2a**) and bis-chelate ($\mathbf{3a^+ClO_4}$) of cobalt(III) crystallize in triclinic $P\bar{1}$ and monoclinic $C2/c$ space group respectively. The molecular view with atom numbering scheme of the complexes $[Co(L^{-I})_3]$ **2a** and $[Co(L^{-I})_2]ClO_4$ $\mathbf{3a^+ClO_4^-}$ are depicted in Fig. 1 and Fig. 2 respectively. X-ray structure of both the complexes revealed that the ligands indeed behave as

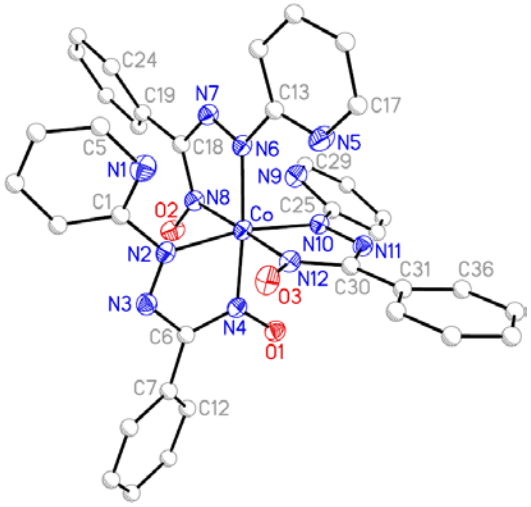

Fig. 1 Molecular view and atom labeling scheme of **2a** (Hydrogen atoms have been omitted for clarity).

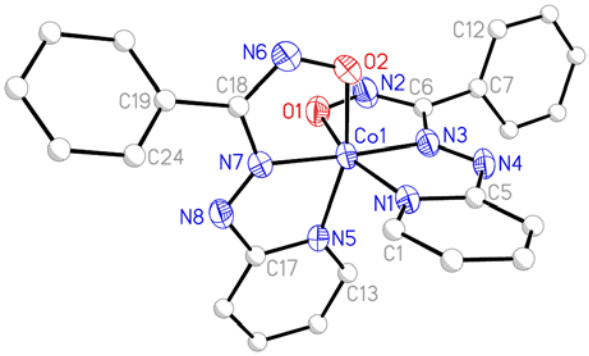

Fig. 2 Molecular view and atom labeling scheme of **3a**$^+$ cation (Hydrogen atoms and counter anion have been omitted for clarity).

flexidentate towards cobalt(III) in homoleplic environment and it binds as tridentate (coordination mode **A**) as well as bidentate one (coordination mode **B**) (Scheme 1). In both cases, the cobalt(III) centers are in a distorted octahedral environment. Three deprotonated ligands L^- (behaving as bidentate uninegative) are coordinated to the metal ion *via* the azo-N and oximato-N in **2a** while the oximato-O is not involved in coordination. Nonetheless in **3a**$^+$**ClO**$_4$, both the deprotonated ligands (behaving as tridentate monoanionic) gets coordinated to cobalt(III) through pyridyl-N, azo-N as well as oximato-O atoms. The coordination of the oximato ligand can be described as tris meidional in **2a** and bis meridional in **3a**$^+$**ClO**$_4$. Notably, the isolation of the facial isomers of both the complexes could not be achieved and this is attributable mainly to steric reasons. In the case of **3a**$^+$, the two coordinated azo-N atoms are lying trans to each other while the disposition of pair of coordinated pyridyl-N as well as oximato-O atoms are cis with respect to each other. Selected metrical parameters of **2a** and **3a**$^+$ are given in Table 1. The three five-membered chelate rings in **2a** are quite planar (average mean deviation 0.028 Å) and the two juxtaposed five-membered rings in **3a**$^+$ (average mean deviation 0.025 Å) are also nearly planar. Two ligands in the bis-clelate **3a**$^+$ are disposed more or less perpendicular to each other (89.3°). The Co–N(azo) lengths in **3a**$^+$ are 1.835(4) Å and 1.841(5) Å respectively and these are appreciably shorter by *ca.* 0.09 Å (average) than that in **2a**. The azo N–N lengths in both the complexes lie in the range 1.26-1.29 Å, as expected in the coordinated azo complexes.[6-11] The N–O (oximato) lengths in the tris complex are significantly shorter (~0.09 Å) as compared to that of the bis complex and this is due to the fact that in the former, oximato-O atoms remain free. The average of the chelate bite angle N(oximato)–Co–N(azo) in **2a** is 80.1°(1). The average N(pyridyl)–Co–N(azo) bite angle in the case of the bis-chelate is

79.7°(2). The bis-chelate contains two ClO_4^- in the lattice i.e., two crystallographically different ClO_4^- ions and the ClO_4^- groups have Cl atom located on special positions so although their crystallographic occupancy at that site is 0.5 (the other half being generated by application of a symmetry element) the chemical occupancy of both Cl groups is one.

Table 1 Experimental Data for Selected Metrical Parameters of **2a** and **3a**$^+$

Bond Lengths (Å)			
2a		**3a**$^+$	
Co1–N2	1.929(2)	Co1–N1	1.942(5)
Co1–N4	1.906(2)	Co1–N3	1.841(5)
Co1–N6	1.933(2)	Co1–N5	1.943(5)
Co1–N8	1.940(2)	Co1–N7	1.835(4)
Co1–N10	1.905(2)	Co1–O1	1.890(4)
Co1–N12	1.908(2)	Co1–O2	1.891(4)
N2–N3	1.288(3)	N3–N4	1.282(6)
N6–N7	1.284(3)	N7–N8	1.262(6)
N10–N11	1.282(3)	C6–N2	1.308 (8)
C6–N4	1.342(3)	C18–N6	1.308(7)
C18–N8	1.353(3)	N2–O1	1.341(6)
C30–N12	1.360(3)	N6–O2	1.343(6)
N4–O1	1.255(3)		
N8–O2	1.253(3)		
N12–O3	1.252(3)		
Bond Angles (°)			
2a		**3a**$^+$	
N2–Co1–N4	80.28(9)	N1–Co1–N3	79.9(2)
N6–Co1–N8	79.75(9)	N5–Co1–N7	79.5(2)
		N1–Co1–O1	162.5(2)
		N5–Co1–O2	162.7(2)

Ground State Geometries and Frontier Molecular Orbital Compositions

Both the **2** and **3**$^+$ complexes are diamagnetic at room temperature indicating their singlet ground state (t_2^6). The geometry optimization of the complexes was performed using their crystallographic coordinates at (R)B3LYP levels in gas phase in their singlet spin state without any ligand simplification. In spite of several attempts, we were unable to grow X-ray quality single crystals of the one electron paramagnetic **3** complex. In an effort to get an insight about the ground state geometry, electronic structure and nature of FMOs of **3**, it was optimized by assuming an S = ½ spin state at (U)B3LYP levels and the optimized structure is given in ESI

(Fig. S2†). The optimized geometries of the synthesized complexes (Ar = Ph) are shown in ESI (Fig. S1†), and the significant metrical parameters are listed in ESI, Table S1†. As depicted in Fig. S1†, the Co(III) atoms adopt a distorted octahedral coordination geometry. The N–N(azo) distance of the free ligand[9] is found to be shorter as compared to their coordinated forms indicating significant population of ligand π* orbital in the diamagnetic homoleptic complexes. The optimized structural parameters of **2a** and **3a**$^+$ are in general agreement with the experimental values and the slight discrepancy (maximum deviation in bond distance: 0.037Å in **2a** and 0.041 Å in **3a**$^+$ for Co–N(azo) length) arises due to the crystal lattice distortion existing in real molecules. Unlike other bond parameters, the N–N(azo) length of **3a**$^+$ and **3a** in their ground state optimized geometries differs appreciably by 0.031 Å signifying substantial contribution of π*(azo) in the spin bearing orbital of radical compound. Isodensity plots of some selected orbitals of the Co(III) complexes are depicted in Fig. 3. The partial frontier molecular orbital compositions and energy levels of some selected orbitals (H − 5 to L + 5) for the cobalt complexes **2a** and **3a**$^+$ along with the HOMO−LUMO energy gap, are listed in Table 2. The superior stabilization of both HOMO and LUMO as well as appreciable reduction in the energy gap between them (~0.5 eV) in case of bis chelates **3a**$^+$ relative to **2a** (Fig. 4), plausibly arises from the better sharing of delocalized π-electrons within the coordinated ligands (Fig. 3). Notably, the contribution of cobalt AOs in these MOs is insignificant. Similar data for anion radical complex **3** are listed in ESI (Table S2†). Comparison of the relative energy levels of FMOs of **2a**, **3a**$^+$ and **3a** are depicted in Fig. 4.

The LUMO of the titled ligand (Ar = Ph) is expected to be stabilized substantially relative to that of the well known dimethylglyoxime ligand due to the presence of azo and pyridyl moieties in conjugation with oxime function and provides superior Co(t_2)→L(π*) back π-donation in the former ligand. The HOMO and LUMO of both the diamagnetic compounds in their ground states are essentially composed of π and π* of coordinated ligand orbitals respectively. Major contribution of HOMO of these molecules arises from π(phenyl) and π(oximato-NO) while that of LUMO primarily comprises the π*(azo) and π*(oximato-NO) in company with π*(pyridyl). As expected, composition of LUMO of diamagnetic **3a**$^+$ is essentially similar with that of HOMO (α - MO) of anion radical **3a**. Notably, the LUMO of **3a**$^+$ is

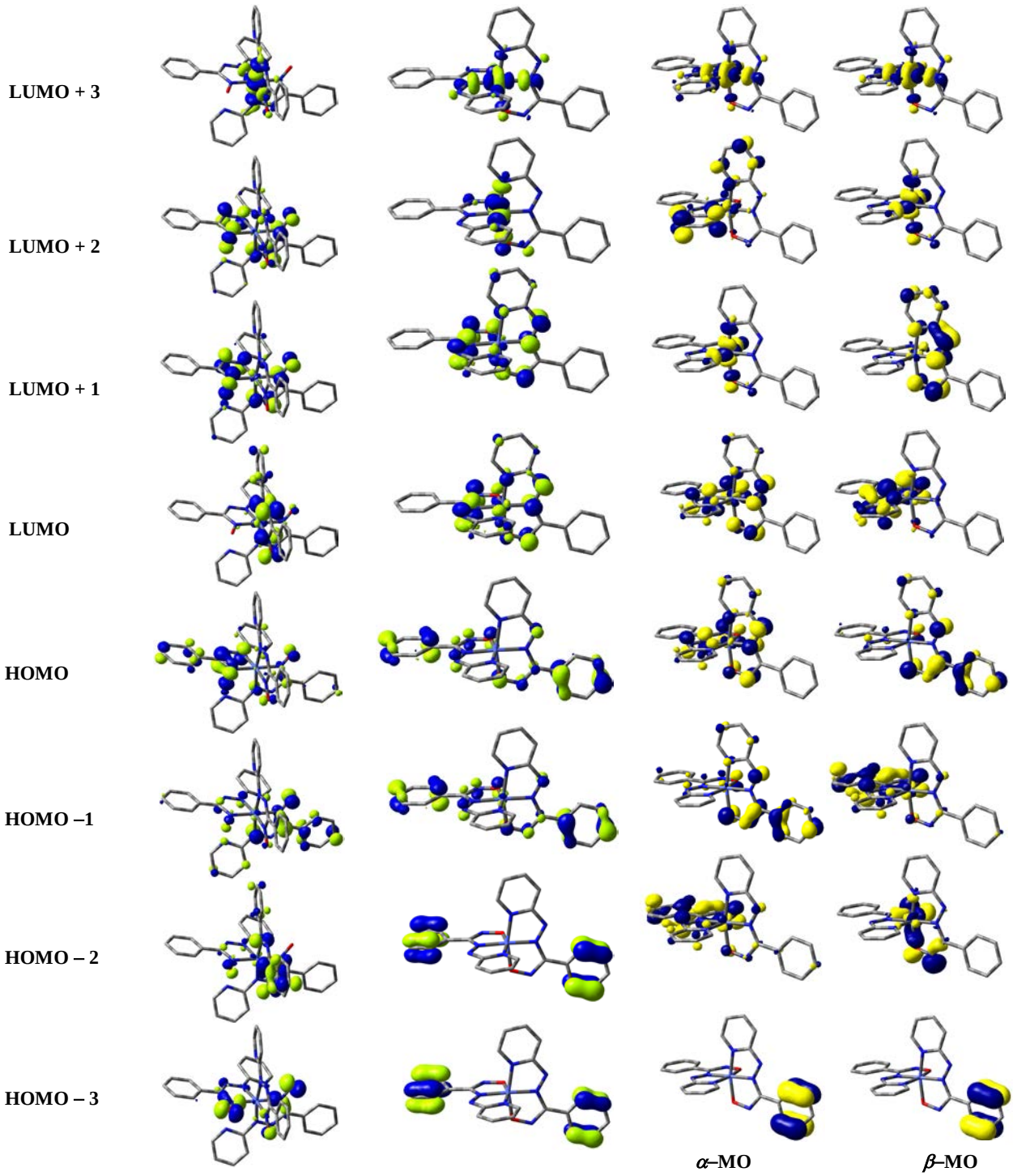

Fig. 3 Isodensity surface plots of some selected frontier molecular orbitals for the complexes **2a**, **3a**$^{+}$ and **3a** at their optimized S_0 geometry in gas phase. Isodensity value 0.05 e Bohr^{-3}.

Table 2 Frontier Molecular Orbital Composition (%) in the Ground State for **2a** and **3a**$^{+}$

Complex	Orbital	MO	Energy (EV)	Contribution (%) Co	Py	Azo	NO	Bz	Main Bond Type
2a	190	L+5	-0.91	1	45	4	10	40	π*(L)
	189	L+4	-1.54	55	2	7	31	5	$d_{x^2-y^2}$(Co) + π*(L)
	188	L+3	-1.66	58	6	25	9	2	d_{z^2}(Co) + π*(L)
	187	L+2	-2.68	1	15	41	42	1	π*(L)
	186	L+1	-2.87	3	14	39	43	1	π*(L)
	185	L	-3.07	3	14	39	42	1	π*(L)
	184	H	-5.52	0	12	14	27	46	π(L)
	183	H–1	-5.56	2	15	15	22	46	π(L)
	182	H–2	-5.71	2	12	12	26	47	π(L)
	181	H–3	-6.06	1	1	8	77	12	π(L)
	180	H–4	-6.58	3	5	9	59	24	π(L)
	179	H–5	-6.64	0	0	0	1	99	π(L)
	HOMO–LUMO gap = 2.45 eV								

	Orbital	MO	Energy (EV)	Contribution (%) Co	Py	Azo	NO	Bz	Main Bond Type
3a^{+}	131	L+5	-4.8	0	95	2	3	0	π*(L)
	130	L+4	-4.89	2	89	3	3	3	π*(L)
	129	L+3	-5.27	59	7	22	8	3	d_{z^2}(Co) + π*(L)
	128	L+2	-5.64	60	16	1	23	1	$d_{x^2-y^2}$(Co) + π*(L)
	127	L+1	-6.86	3	26	39	32	1	π*(L)
	126	L	-6.86	3	27	39	30	1	π*(L)
	125	H	-8.84	0	6	9	18	67	π(L)
	124	H–1	-8.86	2	6	9	16	68	π(L)
	123	H–2	-9.26	0	0	0	0	100	π(L)
	122	H–3	-9.26	0	0	0	0	99	π(L)
	121	H–4	-10.15	7	4	6	61	16	π(L)
	120	H–5	-10.27	7	19	8	41	26	π(L)
	HOMO–LUMO gap = 1.98 eV								

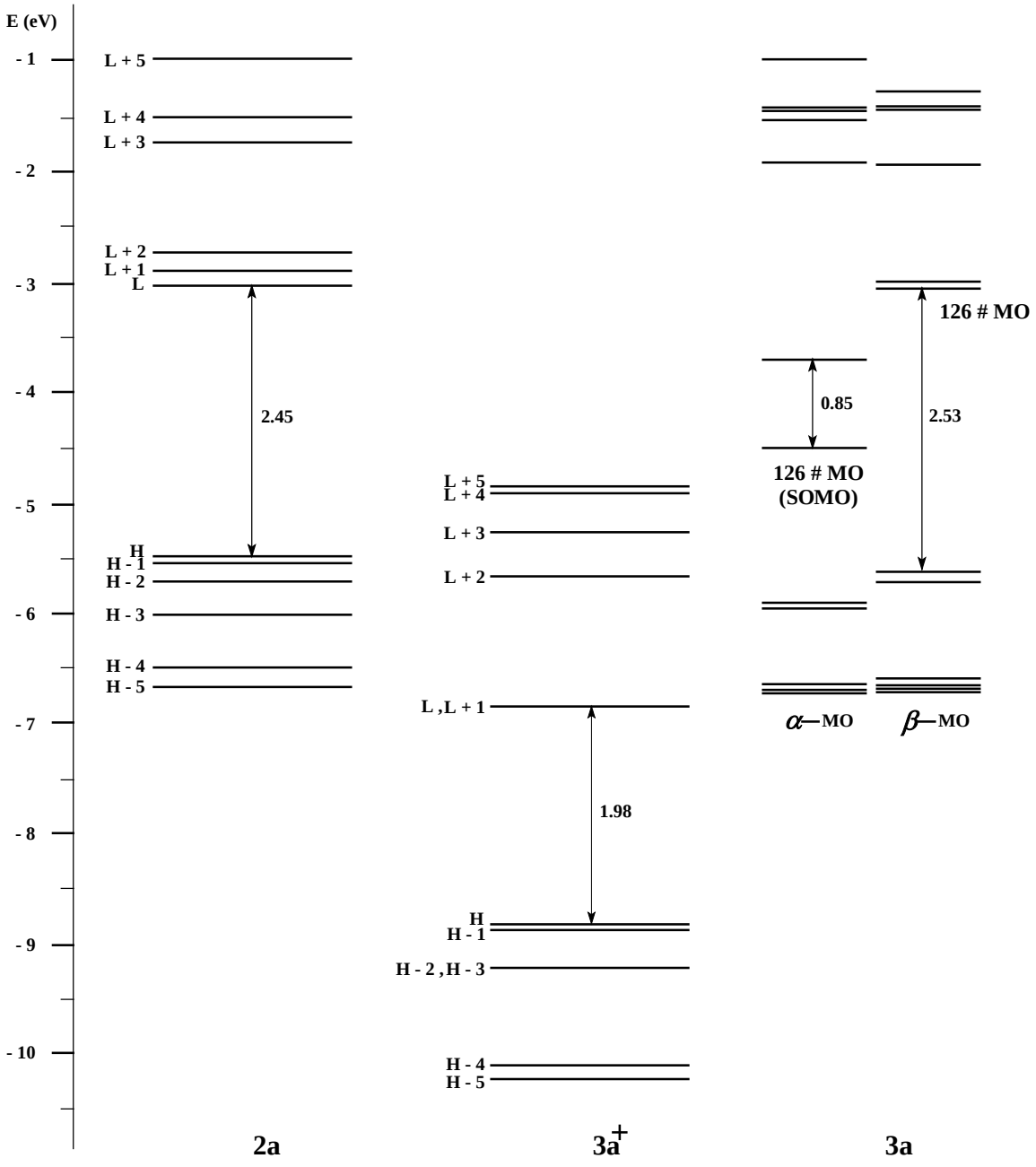

Fig. 4 Partial molecular orbital diagram for complexes **2a**, **3a**$^{+}$ and **3a**. The arrows are intended to highlight the HOMO−LUMO energy gaps. All the DFT energy values are given in eV.

preferentially stabilized in N_4O_2 coordination environment by 3.79 eV relative to **2a** (N_6 coordination) and provides an easy adaptation of an external electron leading to a stable anion radical compound **3a** (Table 2, Fig. 4), which is otherwise unlikely to be achieved. The orbitals of **3a** show the symmetry breaking characteristic of a metal-bound radical complex, with the spin-α and spin-β components of each orbital localized differently in the molecule. The singly

occupied spin-α orbital encompasses equally over both the coordinated ligands (~48% on each L) and lies ~1.43 eV below its vacant spin-β counterpart, which is localized (~93% on one L) primarily on one such ligand (Fig. 3). The more symmetrical distribution of unpaired spin in the occupied spin-α orbital relative to vacant spin-β component reflects the more diffuse nature of the singly occupied orbital in anion radical **3a**. Thus the superior stabilization of the unpaired spin on the ligand array rather than metal confers the reduction event can primarily be viewed as being ligand based. The compositions of HOMO and LUMO are useful in understanding the nature of transitions in the absorption spectra of the complexes as well as the redox behaviour of coordinated ligand (*vide infra*).

Spectral Studies

^{1}H NMR

Both the complexes of type **2** and **3$^+$ClO$_4^-$** and are low-spin t_2^6 diamagnetic systems [S = 0] in pseudo-octahedral geometry, attributable to the comparatively small spin pairing energy of cobalt(III).[13] They are soluble in polar organic solvents such as ethanol, acetonitrile, dichloromethane, chloroform, acetone and so forth, furnishing brown and violet solutions respectively. ^{1}H NMR spectra of these compounds along with the ligand have been recorded in $CDCl_3$ and the spectra are given in ESI (Fig. S3–S5†). The ranges of proton signals for the free ligand **1** and coordinated ligand appeared almost in the similar region. The aromatic region (δ 7.4–8.5 and δ 7.2–8.5 in bis and tris complexes respectively) is rather complex in nature owing to overlap of signals arising from multiple pyridyl and phenyl protons. The differences in chemical shift values in the two homoleptic complexes can be attributed to the different π acceptor ability of azo, oximato and pyridyl groups of **1** in bis and tris chelating environments. Absence of the oximato proton signal (appears as a distinct singlet at δ = 8.8 ppm in the free ligand) in complexes authenticates the coordination of oximato-O atom.

Absorption Spectra

Electronic spectra of the complexes of type **2a** and **3a$^+$ClO$_4^-$** have been recorded in acetonitrile at room temperature and depicted in Fig. 5 while the corresponding spectrum of the free ligand **1a** is presented in ESI (Fig. S6†). Multiple low-energy transitions are the characteristics of the spectra and these excitations are supposed to be primarily due to charge-transfer transitions

within the pyridyl-azo-oximato ligands. The spectral patterns of two types of compounds are similar except for the fact that greater number of transitions is observed for bis-chelates in the visible region. Absorption spectrum of anion radical **3a** complex is depicted in ESI (Fig. S7†). The observed spectrum of **3** appears almost similar to that of its one-electron oxidized form $\mathbf{3}^{+}$ except the absence of some transitions around 400 nm. To gain deeper insight into the electronic properties of the transitions involved in the optical absorption processes, we investigated the synthesized complexes by means of time-dependent density functional theory (TD-DFT) in CH_3CN solvent using CPCM model (see Computational Method for details). The computed vertical transitions were calculated at the equilibrium geometry of the S_0 state and described in terms of one-electron excitations of molecular orbitals of the corresponding S_0 geometry. The most relevant transitions involved along with their energy, character, oscillator strengths computed in solvent and their assignments as well as experimental results of compounds **2a** and $\mathbf{3a}^{+}$are listed in ESI, Table S3† and Table 3 respectively (the similar data for anion radical **3a** is given in ESI, Table S4†). The calculated transitions with moderate intensities ($f \geq 0.02$) can be envisaged going from the lower to the higher energy region of the spectrum. The comparison between the experimental spectra and computed vertical transitions for the complexes **2a**, $\mathbf{3a}^{+}$ and **3a** are depicted in Fig. 5 and ESI, Fig. S7†.

For tris-chelate **2a**, starting from the HOMO and going to more stabilized energies, HOMO − 1, HOMO − 2 and HOMO − 3 are encountered and involve exclusively the delocalized π-orbitals over pyridyl-azo-oximato ligands; the first three molecular orbitals comprise essentially analogous composition *viz*. mainly phenyl ring with moderate contribution of oximato-NO group and a little involvement of azo-π and pyridyl-π orbitals. Notably, HOMO − 3 encompasses exclusively the oximato-NO with small phenyl-π and azo-π orbitals of coordinated ligands. On the other hand, the first three vacant orbitals *viz*. LUMO, LUMO + 1 and LUMO + 2 composed of π* orbitals delocalized mostly over the oximato-NO and azo groups with little involvement of pyridyl moiety. Significantly, LUMO + 3 has major participation of cobalt $3d_z^2$ orbital with minor sharing of azo-π* and oximato-NO-π* orbitals.

As far as the tris-complexes are concerned, several transitions with oscillator strength ($f \geq 0.02$) can be envisaged going from the lower to the higher energy region of the spectra. The low energy transitions are observed near 550 nm as broad band. This feature present in the experimental absorption spectra in the visible region (λ_{abs} = 544) is analysed and it is in excellent

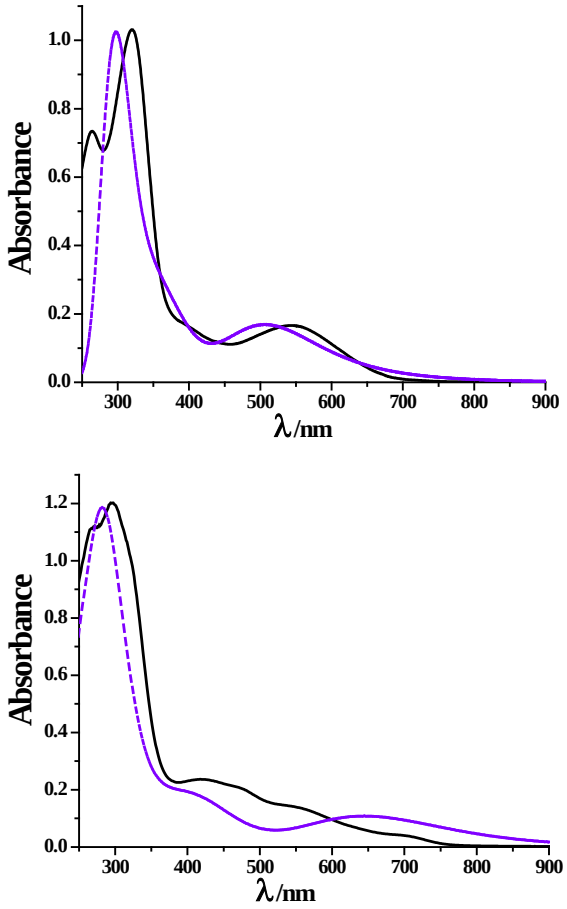

Fig. 5 Experimental (Black bold line) and theoretical (Blue dotted line) absorption spectra of **2a** (top) and **3a**$^{+}$ (bottom) in acetonitrile.

agreement with the absorptions at 539 nm (2.2988 eV, f = 0.0268), 509 nm (2.4376 eV, f = 0.1194) and 507 nm (2.4485 eV, f = 0.0371). Among these three calculated excitations, the first one can be described in terms of a linear combination of the H − 3 → L + 2 (36%), H − 2 → L (14%) and H → L + 2 (11%) character and it is assigned primarily to {[π(phenyl) + π(oximato-NO)] → [π*(azo) + π*(pyridyl)]}, while the second appeared as linear combination of the H − 1 → L + 2 (27%), H → L + 2 (21%) and H − 1 → L + 1 (18%) character and it is assigned to {π(phenyl) → [π*(azo) + π*(oximato-NO)]} transition and the third is basically a linear combination of the H − 4 → L (20%), H − 1 → L + 2 (17%) and H − 3 → L (12%) character and it is assigned to {π(phenyl) → [π*(azo)} transition. Theoretical analysis of these three transitions revealed that they are essentially LLCT/ILCT in nature. The shoulder near 400 nm can be

correlated to the theoretical transitions at 378 nm (3.2786 eV, *f* = 0.0278), 372 nm (3.3310 eV, *f* = 0.0662) and 368 nm (3.3664 eV, *f* = 0.0357). The former excitation can be described as linear

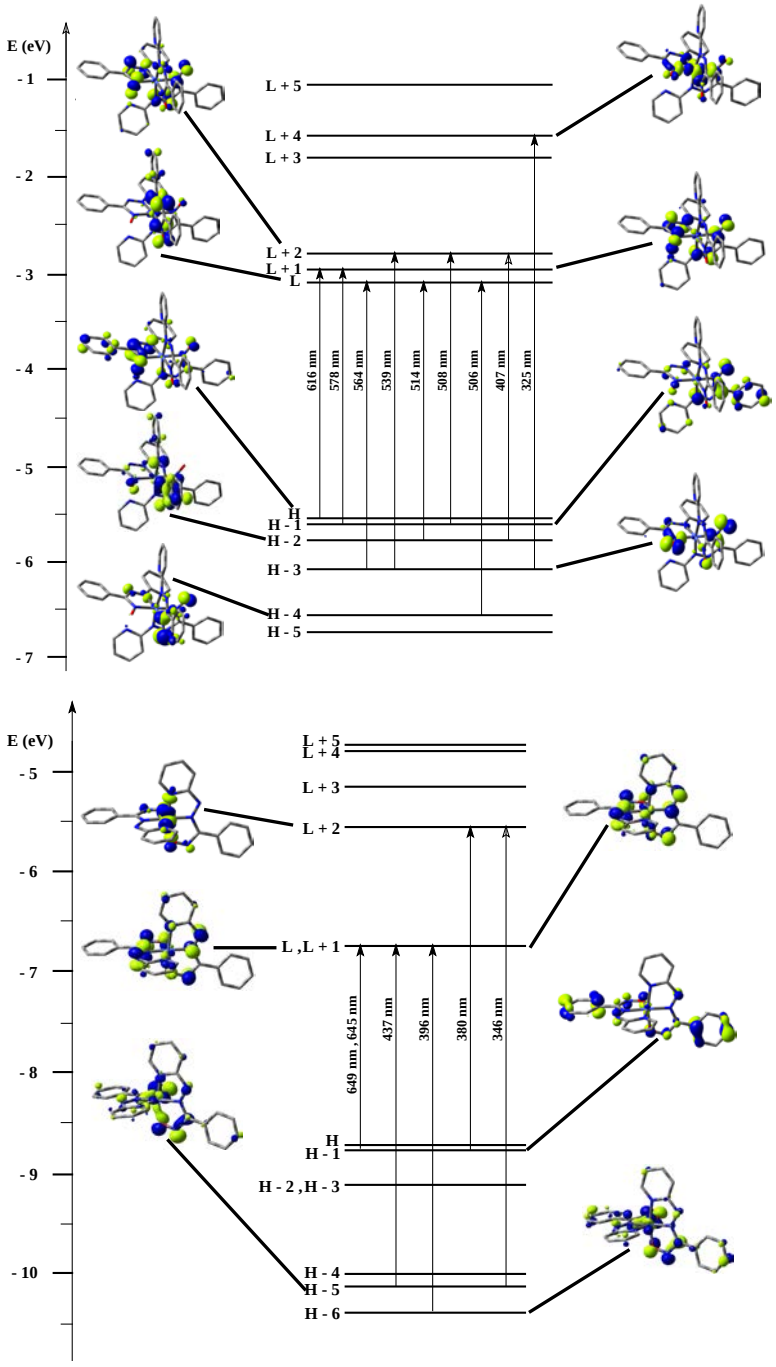

Fig. 6 Partial molecular orbital diagram related to the absorption of complex **2a** (top) and **3a**$^{+}$ (bottom) with some selected isodensity frontier molecular orbital mainly involved in the electronic transitions.

combination of H − 10 → L (57%) character and it is assigned to {[π*(pyridyl)] + π(phenyl)] → [π*(oximato-NO) + π*(azo)]}. The latter two can be ascribed to the H − 8 → L + 2 (27%) transition attributed to {[π*(pyridyl)] + π(phenyl)] → [π*(azo) + π*(oximato-NO)]} excitation and linear combination of H − 9 → L + 1 (25%) and H − 8 → L + 1 (21%) with {[π*(pyridyl)] + π(phenyl)] → [π*(azo) + π*(oximato-NO)]} excitation. The trio of them are of essentially transition with LLCT/ILCT character. The observed absorption in the UV region at 319 nm comprises of the excitation at 325 nm (3.8140 eV and *f* = 0.1607), 295 nm (4.2075 eV and *f* = 0.4497), 294 nm (4.2262 eV and *f* = 0.3248) and 290 nm (4.2686 eV and *f* = 0.2640). The first transition is due to the H − 3 → L + 4 (31%) transition and can be ascribed to {[π(phenyl) + π(pyridyl) + π(oximato-NO)] → [$d_{x^2-y^2}$(Co) + π*(azo)]} transition mainly of LLCT/ILCT character with admixture of LMCT. The second transition is attributed to H → L + 6 (31%) and can be ascribed to {[π(phenyl) + π(pyridyl)] → [π*(oximato-NO) + π*(azo)]} transition largely of LLCT/ILCT character. The third transition is principally the H → L + 6 (37%) transition and can be ascribed to {[π(phenyl) + π(pyridyl)] → [π*(oximato-NO) + π*(azo)]} transition mostly of LLCT/ILCT character. The last one appeared as linear combination of H − 2 → L + 5 (21%) and H → L + 7 (14%) and can be assigned to {π(phenyl) → [π*(azo) + π*(oximato-NO) + $d_{x^2-y^2}$(Co)]} transition having primarily LLCT/ILCT character with little admixture of LMCT. In Fig. 6 reported the schematic representation of the energy levels of molecular orbitals involved in the electronic transitions of **2a** and **3a**$^+$, and that of **3a** is depicted in ESI (Fig. S8†).

For bis-chelates **3**$^+$, starting from the HOMO and going to more negative energies, HOMO − 1, HOMO − 2 and HOMO − 3 are encountered and involve exclusively the delocalized π-orbitals over pyridyl-azo-oximato ligands; the first two molecular orbitals comprise more or less similar composition *viz*. mainly phenyl ring with moderate contribution of oximato-NO group and a little involvement of azo π orbital. The remaining two MOs encompass exclusively the phenyl π orbitals of coordinated ligands. Among the first four virtual orbitals, doubly degenerate LUMO and LUMO + 1 show comparable contribution of azo, pyridyl and oximato groups with the former having superior involvement. On the other hand, the LUMO + 2 and LUMO + 3 have major involvement of cobalt $3d_{x^2-y^2}$ and $3d_{z^2}$ orbital respectively along with minor participation of ligand π* orbital.

For bis-complexes **3a**$^{+}$ several transitions with oscillator strength ($f \geq 0.02$) can be envisaged going from the lower to the higher energy region of the spectra. The low energy transitions are observed near 650 and 450 nm. The first transition with sizable intensity that can be encountered at lower energy is computed at 649 nm (1.9108 eV, $f = 0.0769$) and essentially

Table 3 Main optical transition at the TD-DFT/B3LYP/6-31G Level for the complex **3a**$^{+}$ with composition in terms of molecular orbital contribution of the transition, Computed Vertical excitation energies, and oscillator strength in acetonitrile

	Composition	E (eV)	Oscillator strength (*f*)	λ_{theo} (nm)	Assignment	λ_{exp} (nm)
1.	H – 1 → L + 1 (51%) H → L (45%)	1.9108	0.0769	648.85	ILCT/LLCT	
2.	H – 1 → L (51%) H → L + 1 (44%)	1.9207	0.0643	645.52	ILCT/LLCT	~650 (sh)
3.	H-5 → L (55%) H – 4 → L + 1 (36%)	2.8336	0.0923	437.56	ILCT/LLCT	~450 (sh)
4.	H – 7 → L + 1 (34%) H – 8 → L + 1 (21%) H – 5 → L + 1 (16%)	3.2122	0.0635	385.98	ILCT/LLCT	
5.	H – 4 → L + 2 (30%) H – 5 → L + 3 (24%)	3.5743	0.0709	346.88	LMCT	
6.	H – 6 → L + 2(22%) H – 1 → L + 5 (17%)	4.0977	0.1081	302.57	LMCT/ILCT/LL	
7.	H – 12 → L + 1 (48%) H – 7 → L + 3 (15%)	4.2369	0.1308	292.63	ILCT/LLCT	292

consists of the combination of H − 1 → L + 1 (51%) and H → L (45%). The next intense process is calculated at 645 nm (1.9207 eV, $f = 0.0643$) with H − 1 → L (51%) and H → L + 1 (44%) character. The more intense and higher energy feature present in the experimental absorption spectra in the visible region (λ_{abs} = 470 and 410 nm) is analysed and it is in good agreement with the absorptions at 437 nm (2.8336 eV, $f = 0.0923$) and 386 nm (3.2122 eV, $f = 0.0635$). The

former excitation can be described in terms of linear combination of the H − 5 → L (55%) and H − 4 → L + 1 (36%) and it is assigned to {[π(phenyl) + π(oximato-NO)] → [π*(azo) + π*(pyridyl)]} transition while the latter one is attributed to the combination of H − 7 → L + 1 (34%), H − 8 → L + 1 (21%) and H − 5 → L + 1 (16%) and it is assigned to {π(phenyl) → π*(azo) + π*(pyridyl) + d_z^2(Co)} transition and both of them are of mainly LLCT/ILCT character. The low energy absorptions near 330 nm (sh) in the UV region are computed at 347 nm and 303 nm. The first transition with sizable intensity at 347 nm (3.5743 eV, *f* = 0.0709) and essentially consists of the combination of H − 4 → L + 2 (30%) and H – 5 → L + 3 (24%) and can be ascribed to {[π(phenyl) + π(oximato-NO)] → [$d_{x^2-y^2}$(Co) + d_z^2(Co)]} transition. The other intense process is calculated at 303 nm (4.0977 eV, *f* = 0.1081) with H − 6 → L + 2 (22%) and H – 1 → L + 5 (17%) character and can be attributed to {π(phenyl) → [$d_{x^2-y^2}$(Co) + d_z^2(Co) + π*(pyridyl)]} transition. As a whole, the observed excitation near 330 nm can best be described as mostly phenyl(π) to metal(e) i.e., LMCT transition. The absorption in the UV region at 292 nm comprises of the excitation at 293 nm (4.2369 eV and *f* = 0.1308). The transition is due to the contribution of H − 12 → L + 1 (48%) and H − 7 → L + 3 (15%) and can be ascribed to {[π(phenyl) + π(pyridyl)] → [π*(azo) + π*(oximato-NO)]} transition mainly of LLCT/ILCT.

For both the Co(III)-pyridyl-azo-oxime systems, occupied molecular orbitals closer to the frontier region show strongly mixed π character of the coordinated ligand as scrutinized by the theoretical analysis while the virtual FMOs comprise primarily ligand π* with some admixture of cobalt $3d_z^2$ and $3d_{x^2-y^2}$ AOs for **2** and exclusively ligand π* for $\mathbf{3}^+$ respectively. In the visible region, all the computed excitations can be best described as a mixed singlet-manifold Intra-ligand charge-transfer (^{1}ILCT) and ligand-ligand charge-transfer (^{1}LLCT) transitions, with different amount of π−π* character within the coordinated pyridyl-azo-oximato ligands, for both types of complexes. In the higher energy region (UV), similar considerations can be brought for the bis-complexes $\mathbf{3}^+$ i.e., all the excitations are essentially due to ILCT/LLCT transitions as found from theoretical calculation. On the contrary for tris-complexes **2**, the excitations in this region can be assigned as π−π* ILCT/LLCT transitions with some admixture of LMCT component.

In our effort to unveil the underlying electronic properties of the transitions involved in the optical absorption processes of the anion radical compounds, we optimized the geometry of **3a** followed by the analysis with the aid of time-dependent density functional theory (TD-DFT)

in CH_3CN solvent using CPCM model. Transitions with oscillator strength ($f \geq 0.02$) can be envisaged going from the visible to the UV region of the spectrum. The low energy band is found theoretically near 600 nm. The lowest energy transition with sizable intensity that can be encountered, is computed at 630 nm (1.9669 eV, f = 0.0629) and it essentially consists of the combination of H − 1 → L (α) (30%) and H → L + 1 (β) (54%). The next intense process is calculated at 618 nm (2.0038eV, f = 0.0711) with H − 2 → L (α) (36%) and H – 1 → L (β) (49%) character. The higher energy feature present in the experimental absorption spectra in the visible region (λ_{abs} = 535 nm (sh)) is analysed and it is in good agreement with the absorptions at 516 nm (2.4040eV, f = 0.0219) and 512 nm (2.4219 eV, f = 0.0102). The former excitation can be described in terms of linear combination of H → L + 3 (α) (50%), H – 2 → L (β) (14%) and H – 6 → L (α) (10%) while the latter one is attributed to the combination of H → L + 3 (α) (27%), H − 5 → L (β) (24%) and H − 2 → L (β) (10%). Both the transitions are assigned to {[π(oximato-NO)] + π(phenyl)] → [d_z^2(Co) + π*(azo) + π(pyridyl)]} and they are mainly of MLCT character with little LLCT/ILCT contribution. The experimental absorption spectra in the UV region (λ_{abs} = 292 nm) is analysed and found to be consists of four vertical transitions. The first transition at 307 nm (4.0398 eV, f = 0.0943) is due to the contribution of H − 1 → L + 3 (α) (51%) and can be ascribed to {[π(phenyl) + π(oximato-NO)] → [d_z^2(Co) + π*(azo)]} transition mainly of MLCT/LLCT/ILCT character. The second transition at 304 nm (4.0818 eV, f = 0.1003) is owing to the contribution of H − 2 → L + 3 (α) (38%) and H − 1 → L + 4 (β) (22%) and can be assigned to {[π(phenyl) + π(oximato-NO)] → [π*(azo) + π*(pyridine)]} transition mainly of LLCT/ILCT character. Another transition at 299 nm (4.1503 eV, f = 0.0379) is due to the contribution of H → L + 9 (α) (18%) and H − 1 → L + 4 (α) (10%) and can be attributed to {[π(phenyl) + π(oximato-NO)] → [π*(azo) + π*(pyridyl)]} transition mainly of LLCT/ILCT character. The last one at 297 nm (4.1694 eV, f = 0.0255) is because of the contribution of H − 1 → L + 4 (α) (15%) and H → L + 9 (α) (11%) and can be ascribed to {[π(phenyl) + π(oximato-NO)] → [π*(azo) + π*(pyridyl)]} transition mainly of LLCT/ILCT character. Thus the overall assignment of the anion radical **3** can be best demonstrated as essentially MLCT with some admixture of LLCT/ILCT in the visible region while that in the UV region it appears to be exclusively of LLCT/ILCT character.

Luminescence Spectra

The emission spectral behaviour of the complexes of type **2a** and **3a**$^{+}$ were studied at room temperature in acetonitrile solution. Both type of complexes upon excitation at the wavelengths, where their ^{3}ILCT/LLCT admixed with ^{3}LMCT absorption maxima were observed, exhibit broad luminescent maxima near 400 nm (shown in Fig. 7) and these remain unaffected with the energy of excitation wavelengths. The reported oximato complexes of cobalt(III) are found to be moderate emitters (quantum yields (Φ) = 3.5-5.1 × 10^{-3}). Table 4 summarizes the emission maxima (λ_{em}), quantum yield (Φ), lifetime (τ), radiative (k_r) and nonradiative (k_{nr}) decay rate constants (ESI, Fig. S11†). The luminescence spectrum and the time-resolved photoluminescence decay of **1b** are presented in ESI (Fig. S9 and S10†). Notably, luminescence study of complexes with ligands containing pyridyl-azo moiety is less common.[14]

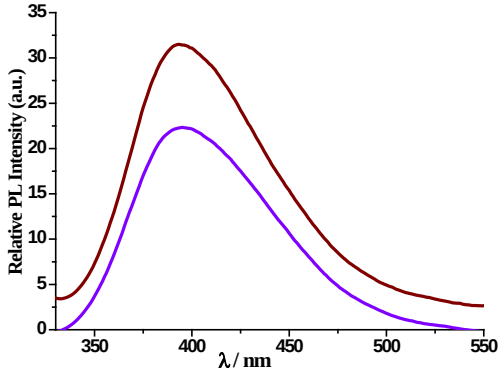

Fig. 7 Luminescence spectra of complexes **2a** (blue) and **3a**$^{+}$ (brown) in acetonitrile at room temperature.

Table 4 Luminescence spectral data[a] for **1, 2** and **3**$^{+}$ in acetonitrile at room temperature

Ligand	Complex	λ_{em} (nm)	τ (ns)	Φ (×10^{-3})	k_r, s^{-1} (×10^{5})	k_{nr}, s^{-1} (×10^{8})
1a		398	6.73	10.287	15.282	1.471
1b		398	6.70	10.274	15.334	1.477
	2a	396	6.63	3.782	5.704	1.503
	2b	394	5.92	3.550	5.997	1.683
	3a^{+}	393	6.61	5.099	7.714	1.505
	3b^{+}	393	6.34	4.629	7.301	1.570

[a]The compounds **1**, **2** and **3**$^{+}$ are excited at 283 nm, 319 nm and 292 nm respectively.

In order to investigate the geometrical rearrangement as well as to understand the electronic nature of the emitting excited state, geometrical optimization of the lowest lying triplet-manifold excited state (T_1) was performed by means of DFT using the unrestricted Kohn−Sham approach (UKS) at (U)B3LYP/(6-31G + LANL2DZ) level. The most meaningful geometrical parameters for the reported cobalt(III)-oximato compounds are listed in ESI, Table S1†. The isodensity surfaces of the Highest and Lowest Singly Occupied Molecular Orbitals, *viz*. HSOMO and LSOMO, at the relaxed T_1 geometry are depicted in Fig. 9. In addition, the corresponding electron spin density, which is defined as the difference between α and β spin contributions to the total electron density at the T_1 optimized geometry are also illustrated in Fig. 9. The tris-chelate **2a** displays comparable metrical parameters for Co−N(oxime) and Co−N(azo) linkages and N(azo)−Co−N(oxime) angle at the T_1 optimized geometry as well as in the S_0 state (average displacement range 0.002−0.005 Å and 0.25° respectively) (ESI, Table S5†). The bis-chelate **3a**$^+$ also exhibits marginal differences in Co−N(py), Co−N(azo) and Co−O(oxime) bond distances and N(azo)−Co−N(py) and N(azo)−Co−N(oxime) bond angles at the T_1 optimized geometry with respect to that of S_0 state (average displacement range 0.001−0.007 Å and 0.04−0.21° respectively) (ESI, Table S5†). It is noteworthy that the N−N(azo), N−O(oximato) and C−N(oximato) bond distances of tris chelate **2a** remain practically same in two ligands while there is a significant lengthening of N−N(azo) and N−O(oximato) by 0.072 Å and 0.036 Å respectively have been found in the third ligand in the T_1 state relative to that in the S_0 state (ESI, Table S1†). Analogous lengthening of N−N(azo) and N−O(oximato) bond lengths in one ligand is also observed for bis chelate **3a**$^+$ (ESI, Table S1†). The absence of appreciable distortion around the cobalt center signifies that the population of the T_1 state results in only minor deviations in the geometrical arrangement of the coordination spheres i.e., metal-ligand interactions have hardly been altered during $S_0 \rightarrow T_1$ excitation. This is consistent with the comparable quantum yield (Φ) of the synthesized cobalt(III) complexes with that of free ligand (Table 4). Nonetheless, quantum yield (Φ) is diminished to some extent in cobalt(III) complexes relative to the free ligand **1** and this type of quenching of the blue emission of the free ligand may be attributed to the presence of Co(III) center.[7] Quenching process can be attributed due to perturbation of cobalt(III) by partaking of metal-d orbitals into the emissive triplet state (Fig. 10). The considerable geometrical variation is confined essentially to N−N(azo) linkages and to a certain extent in N−O(oximato) bonds of one of the coordinated ligands in the respective

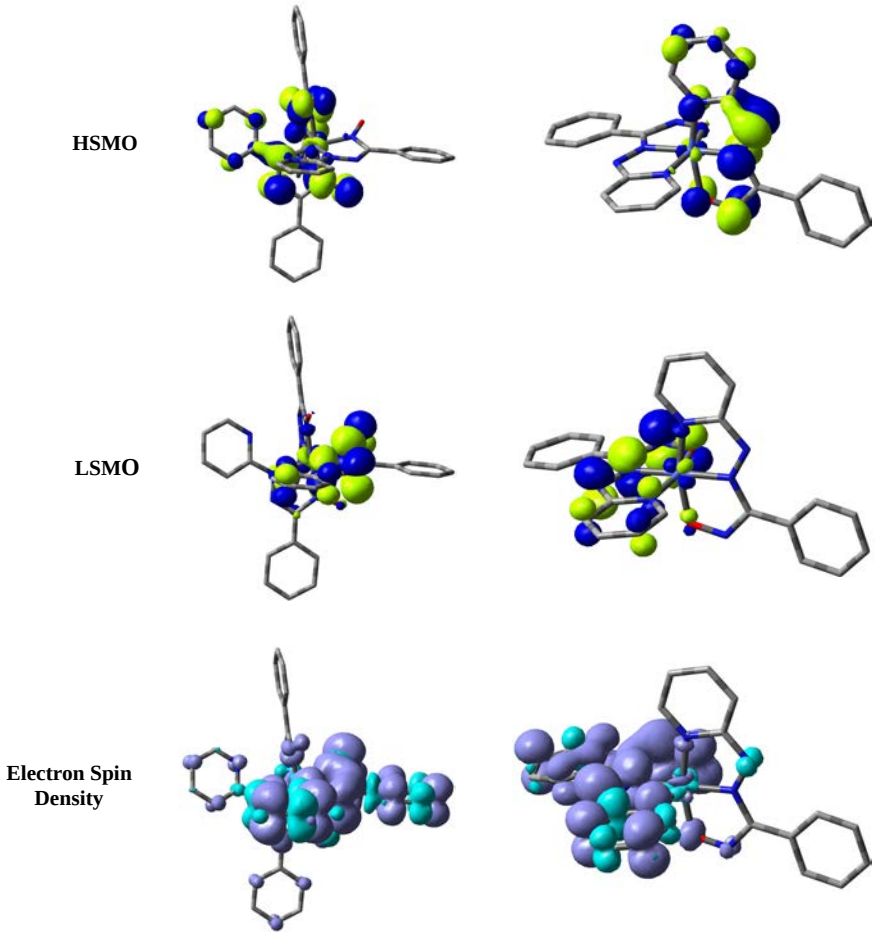

Fig. 9 Isodensity surface plots of the highest and lowest singly occupied molecular orbitals, HSOMO and LSOMO, respectively, along with the corresponding electron spin density for the compounds **2a** and **3a**$^{+}$ at their T_1 geometry. Purple and turquoise colors show regions of positive and negative difference between the alpha and the beta electron densities respectively.

complexes. This can be ascribed to the drifting of electron density mainly from phenyl group to azo and oximato moieties in the excited T_1 state of the coordinated pyridyl-azo-oximato ligand.

Upon analyzing the singly occupied molecular orbitals at the relaxed T_1 geometry for tris chelate it was found that both the LSOMO and HSOMO are located exclusively on the ligand. The LSOMO assumes mainly π(phenyl) with some admixture of [π(oximato) + π(azo) + π(py)] while that of HSOMO comprises of primarily [π(oximato) + π(azo)] along with minor contribution from π(py) (ESI, Table S7†). These singly occupied molecular orbitals resemble the energetically comparable set of orbitals HOMO/HOMO – 1/HOMO – 2 and LUMO/LUMO + 1/LUMO + 2 respectively of the corresponding S_0 equilibrium geometry (Table 2). Similar

studies for the bis chelate also reveal that both the LSOMO and HSOMO are located entirely on the ligand. The LSOMO assumes mostly π(phenyl) with little contribution from [π(oximato) + π(azo)] while that of HSOMO encompasses largely [π(oximato) + π(azo)] along with appreciable contribution from π(py) (ESI, Table S8†). These singly occupied molecular orbitals resemble degenerate HOMO and HOMO – 1 and LUMO/LUMO + 1 (energetically degenerate)

Table 5 Main calculated vertical transitions with compositions, vertical excitation energies and oscillator strength of **2a** and **3a**$^{+}$ in acetonitrile based on the lowest lying triplet excited state

Complex	Excitation	Composition	E (eV)	Oscillator strength (*f*)	λ_{theo} (nm)	Assignment	λ_{exp} (nm)
2a	1.	187 → 184 (11%) 186 → 177 (29%) 188 → 185 (15%)	2.4455	0.0488	507.00	^{3}MLCT/ILCT/LL CT	
	2.	186 → 171 (27%) 186 → 177 (18%)	2.4660	0.0427	502.77	ILCT/LLCT	
	3.	188 → 184 (43%)	2.9854	0.0200	415.30	^{3}MLCT/ILCT	396
3a^{+}	1.	127 → 117 (12%) 130 → 121 (21%)	2.9081	0.0175	426.35	ILCT/LLCT/^{3}MLCT	
	2.	127 → 120 (10%) 128 → 119 (17%)	2.9866	0.0164	415.13	^{3}MLCT/ILCT/LLCT	
	3.	132 → 126 (33%) 129 → 124 (12%) 131 → 126 (10%)	3.2434	0.0132	382.27	^{3}MLCT/ILCT/LLCT	393

respectively of the corresponding S_0 equilibrium geometry (Table 2). In addition, the electron spin density plots for these homoleptic tris and bis chelates disclosed that for all the complexes the spin is located on mainly the pyridyl-azo-oximato ligand.

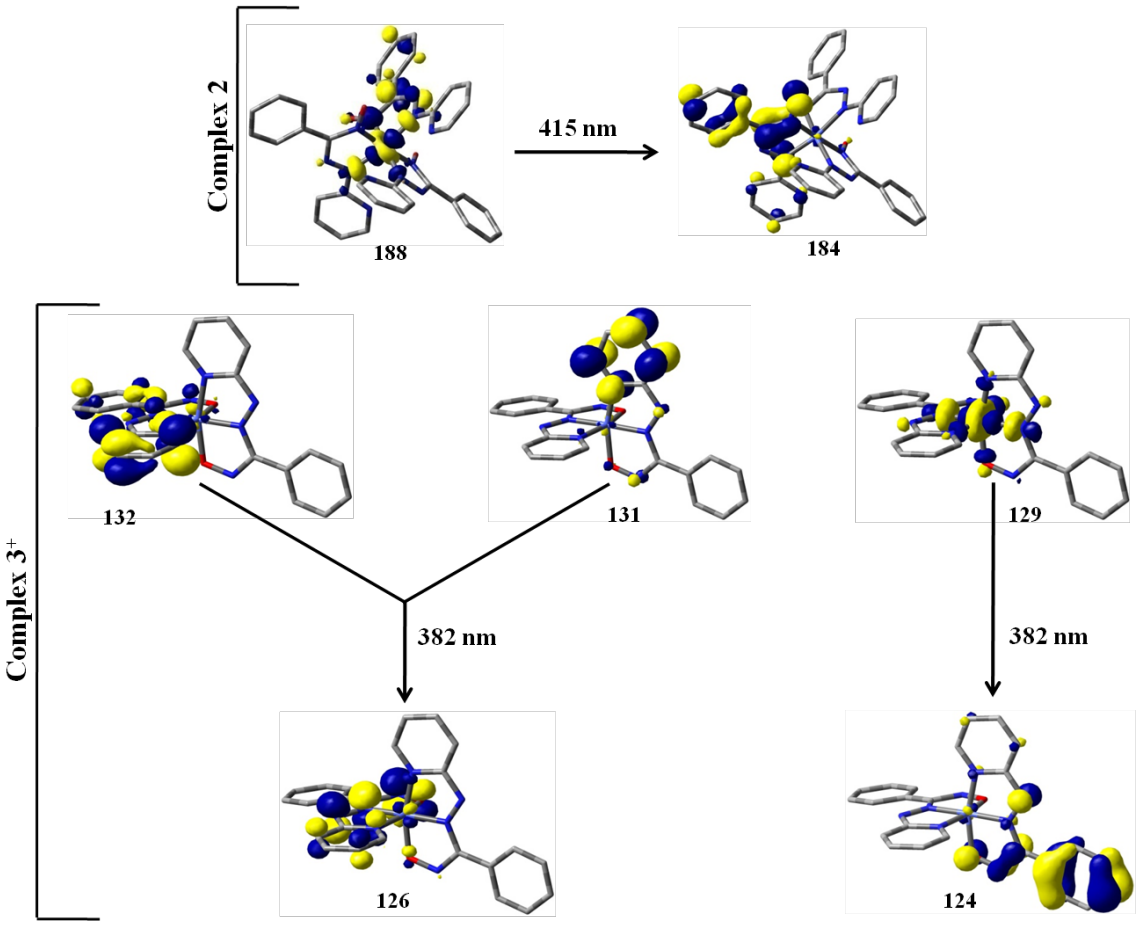

Fig. 10 Frontier molecular orbitals related to emission of **2a** and **3a**$^{+}$.

The observed band of the tris complexes in experimental emission spectrum ($\lambda_{em} \approx 395$ nm) are computed at 415 nm (2.9854 eV, $f = 0.0200$) with significant transition having 188 → 184 (43%) character. This can be assigned exclusively to {d(Co) → π(oximato) + π(pyridyl) + π(aromatic)} ^{3}MLCT transition. The analogous band present in the experimental emission spectrum (λ_{em} = 393 nm) of bis complexes is computed, in excellent agreement, at 382 nm (2.3989 eV, $f = 0.0062$) with 132 → 126 (33%), 129 → 124 (12%) and 131 → 126 (10%) character. This can be assigned to mainly {[π*(pyridyl) + d(Co) + π*(aromatic)] → [π(aromatic) + π(azo) + π(oximato)]} ^{3}MLCT transition mixed with LLCT/ILCT nature. The plots of frontier molecular orbitals associated with the emissions of **2a** and **3a**$^{+}$ are presented in Fig. 10. Consequently, quenching of the emission quantum yield in both types of complexes plausibly originates due to the involvement of cobalt-d orbital in the triplet excited states (Fig. 10; ESI, Table S7 and S8†).

Ligand Redox, EPR and Azo-oxime Anion Radical Complex

Electron-transfer property of the homoleptic tris **2** and bis **3^+ClO_4** cobalt(III) complexes was studied by using cyclic voltammetry in acetonitrile solution (0.1 M NEt_4ClO_4) by using a platinum working electrode (Table 6) at 25 °C. The reported potential is referenced to the Ag/AgCl electrode. The value for the ferrocenium/ferrocene couple, under our experimental conditions, was 0.44 V. The one electron nature of the redox couples have been verified by comparing its current height (i_{pa}) with that of the standard ferrocene-ferrocenium couple under identical experimental conditions.

Table 6 Electrochemical data[a] for tris and bis chelates of cobalt(III) in acetonitrile

Compound	$E_{1/2}$/V (ΔEp/mV)	
	reduction	oxidation
2a	–0.55 (90), –0.90 (100), –1.15	+1.55[b]
2b	–0.58 (90), –0.95 (100), –1.22	+1.51[b]
$3a^+ClO_4$	+0.08(70), –0.42(80)	
$3b^+ClO_4$	+0.05(80), –0.42(90)	

[a]Solute concentration ≈ 10^{-3} mol dm^{-3}; scan rate, 50 mV s^{-1}; $E_{½} = ½(E_{pa} - E_{pc})$ for reversible one-electron process, where E_{pa} and E_{pc} are the anodic and cathodic peak potentials, respectively; $\Delta E_p = E_{pa} - E_{pc}$. [b]$E_{pa}$ value.

Both the complexes of type **2** and **3^+ClO_4** are electro-active in solution (Table 6). The violet complexes of type $[Co^{III}(L^{-I})_3]$ **2** display three successive one electron reductive responses in the region –0.55 V to –1.22 V while brown bis complexes $[Co^{III}(L^{-I})_2]^+$ **3^+** exhibit two such one-electron reductive waves at *ca.* +0.1 and –0.4 V respectively as depicted in Fig. 11. It is noteworthy that unlike the bis chelates, tris chelate exhibits an irreversible anodic oxidative response near +1.6 V. To gain insight into the nature of the redox orbitals, we performed DFT calculation (*vide infra*) for both the homoleptic complexes by optimizing their geometries in acetonitrile solvent. Calculation indicates LUMO, LUMO – 1, LUMO – 2 for the tris chelates **2** and LUMO, LUMO – 1 for the bis chelates **3^+** (ESI, Table S6†) are exclusively distributed over the pyridyl-azo-oximato framework with an appreciable contribution from the azo π* orbital. The irreversible oxidative response in **2** (Table 6) can be attributed to the coordinated ligand oxidation since HOMO is associated with the π orbital that delocalized exclusively over the phenyl and oximato-NO moieties of the coordinated pyridyl-azo-oxime ligand (Table 2, Fig.

3).[15] It is worth noting that the absence of such oxidative response in $\mathbf{3}^{+}$ complexes is nicely corroborated with the superior stability of HOMO of $\mathbf{3}^{+}$ compared to that of **2** (E_{HOMO}(**2a**) = –5.52 eV *vs*. E_{HOMO} ($\mathbf{3a}^{+}$) = –8.89 eV) (ESI, Table S6†).

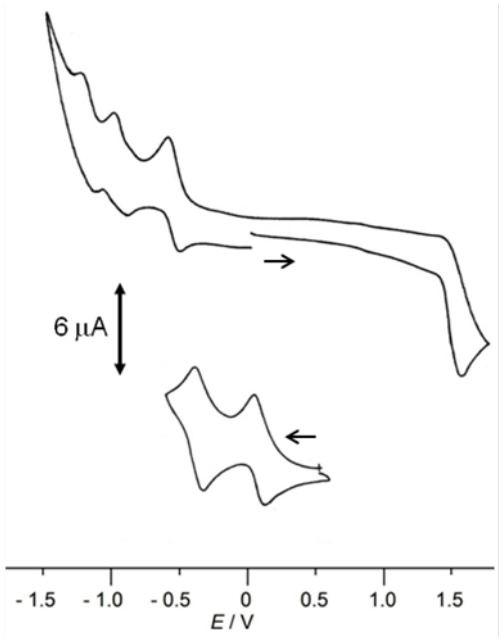

Fig. 11 Segmented cyclic voltammograms of **2a** (top) and $\mathbf{3a}^{+}$ (bottom) in acetonitrile.

The first reductive response occurs at more positive potential (~0.6 V) in case of bis chelates $\mathbf{3}^{+}$ relative to that of **2** signifies considerable stabilization of its LUMO and this provide facile access for the generation of one-electron reduced species since such low-lying redox orbital exhibits superior efficacy to accept an odd electron.[6] Exhaustive constant potential electrolysis of $\mathbf{3}^{+}\mathbf{ClO_4}$ in acetonitrile solution at –0.2 V confirms the transfer of one electron per molecule to obtain a pinkish brown solution. The solution was evaporated immediately to isolate a dark colored solid of composition [$Co^{III}L_2$] **3** in good yield. Notably, the reduced species can also be chemically synthesized by reacting $\mathbf{3}^{+}\mathbf{ClO_4}$ with hydrazine hydrate in acetonitrile solution. The cyclic voltametry of **3** (initial scan cathodic) is virtually the same as that of $\mathbf{3}^{+}\mathbf{ClO_4}$ (initial scan anodic). In the solid state, **3** are indefinitely stable in dry air but the solutions undergo facile oxidation to form the more stable $\mathbf{3}^{+}\mathbf{ClO_4}$. Although we were not able to grow X-ray quality single crystals of **3**, the characterization of the anion radical complexes have been done by spectroscopic techniques. The magnetic moments of **3** ($\mu_{eff} \approx 1.78\ \mu_B$) correspond to one unpaired electron and the complexes are EPR active. They display a broad unresolved signal at *g*

~ 2.0030 in dichloromethane solution at 298 K while in frozen solution (77 K) a sharp EPR signal with eight hyperfine splitted lines (I for ^{59}Co is 7/2) were obtained with $g_{iso} \approx 2.0025$ and hyperfine coupling constant $A \approx 30$ G (Fig. 12).[16] The observed g value is typically that of free-electron and the small cobalt hyperfine coupling indicates that merely a small fraction of the electron spin density from the radical is delocalized toward the cobalt center.

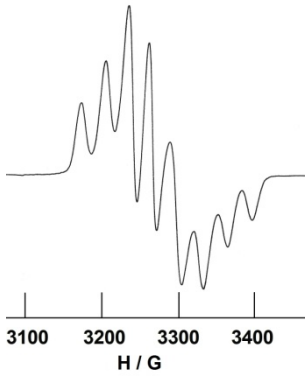

Fig. 12 X-Band EPR spectrum of **3a** in frozen solution (1:1 CH_2Cl_2/toluene) at 77 K. Instrument settings: microwave frequency, 9.11 GHz; modulation frequency, 100 kHz.

The best description of the one-electron paramagnetic **3** can be ascertained as $[Co^{III}\{(L^{-I})_2\}^{\bullet -}]$ from the EPR and DFT studies where the unpaired spin is delocalizes mainly over π^* orbital of both the coordinated ligands (97%) with minor participation (3%) of cobalt d_{yz} orbital (ESI, Fig. S2† and Table S2†). The net spin density of one-electron reduced form **3a** (ρ_L = +0.507 per L, ρ_M = –0.014) is depicted in Fig. 13, implying unambiguously the ligand-based reduction. Ligand centered electrochemical responses *vis-à-vis* stability of metal-bound radical complexes reveal the non-innocent nature of the pyridyl-azo-oxime ligand.

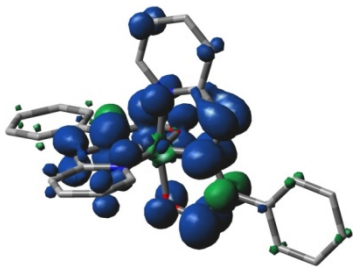

Fig. 13 Net spin density of **3a**. Isodensity value 0.05 e Bohr^{-3}.

Conclusions

We have examined the molecular and electronic structures of the two types of homoleptic complexes **2** (tris chelate) and $\mathbf{3^+ClO_4}$ (bis chelate) with the potential flexidentate pyridyl-azo-oxime ligand **1**. The geometry of both types are authenticated by X-ray diffraction study. The coordination environment of tris and bis chelates is found to be N_6 and N_4O_2 respectively and this strikingly influences the spectral and redox properties of the complexes. Particularly, the superior stabilization of both HOMO and LUMO as well as decrease in the energy gap between them in bis chelates $\mathbf{3^+}$ relative to **2**, can be attributed to the better sharing of delocalized π-electrons within the coordinated ligands.

Both types of compounds display rich spectral features in the UV-vis region. The oximato ligand shows luminescence and its metallo conjugates with Co(III) are found to be moderately blue emissive with slight quenching of the emission quantum yield as compared to that of free ligand. In this context, we have presented combined experimental and theoretical studies of the cobalt(III) complexes. To gain a better insight of the geometry and electronic structures, optoelectronic properties and the nature of the emitting excited state, density functional theory (DFT) and time-dependent DFT (TD-DFT) calculations were performed. This led us to provide a detailed assignment of the significant spectral features of the investigated complexes. The occupied molecular orbitals closer to the frontier region show strongly mixed π character of the coordinated ligand for both **2** and $\mathbf{3^+}$ while the virtual FMOs comprise primarily ligand π* with some admixture of cobalt $3d_z^2$ and $3d_{x^2-y^2}$ AOs for **2** and exclusively ligand π* for $\mathbf{3^+}$ respectively. In the visible region, all the computed excitations can be best described as a mixed singlet-manifold ^{1}ILCT and ^{1}LLCT transitions, with different amount of π−π* character within the coordinated pyridyl-azo-oximato ligands, for both types of complexes. In the UV region, all the excitations are essentially due to ILCT/LLCT transitions for the $\mathbf{3^+}$. In contrast, the allied excitations can best be assigned as π−π* ILCT/LLCT transitions with some admixture of LMCT component for **2**. The observed luminescence band of the tris complex **2** can be assigned exclusively as {d(Co) → π(oximato) + π(pyridyl) + π(aromatic)} ^{3}MLCT transition. The analogous band of $\mathbf{3^+}$ is also in excellent agreement with the computed data and can be attributed to mainly {[π*(pyridyl) + d(Co) + π*(aromatic)] → [π(aromatic) + π(azo) + π(oximato)]} ^{3}MLCT transition along with LLCT/ILCT character. Quenching of the emission quantum yield

in the complexes can be ascribed to the involvement of cobalt-d orbital in the triplet excited state.

Electrochemical investigations on the homoleptic pyridyl-azo-oxime complexes of cobalt(III) reveal a series of reductive responses. DFT calculations authenticate the nature of virtual orbitals associated with the observed redox responses as primarily delocalized π* orbitals of the coordinated pyridyl-azo-oxime. Significantly, the bis chelates $\mathbf{3}^{+}$ exhibit more stabilized vis-à-vis easily accessible nature of LUMO for intake of an extra electron relative to the tris analogues and this fact is consistent with the isolation of single reduced forms **3** in the crystalline state from the diamagnetic $\mathbf{3}^{+}$ precursors. The one electron paramagnetic **3** (S = ½) display sharp eight line EPR spectra with $g \approx 2.0025$ and $A \approx 30$ G indicating their anion radical nature with little cobalt (I of ^{59}Co = 7/2) contribution. Therefore, we have been unambiguously able to establish the concepts of redox non-innocent behaviour of the titled ligands **1** and their ability to form metal-stabilized anion radical complexes when reacted with metal ion having inert t_2^6 configuration. Theoretical study of **3** also confirms the anion radical picture since the spin bearing orbital (α - MO) comprises strongly mixed π* orbital of both the ligands (97%) having more or less comparable contributions from azo, oximato-NO and pyridyl functions along with little participation of metal-d_{yz} (3%). Thus, the best description of **3** can be viewed as $[Co^{III}\{(L^{-I})_2\}^{\bullet -}]$ from both theoretical and experimental studies. To the best of our knowledge these are the first examples of cobalt (III)-stabilized azo-oxime anion radical complexes.

Experimental details

General

The chemicals used were purchased from the following sources: 2-hydrazinopyridine from Aldrich Chemical Co., Limited, benzaldehyde, n-butyl amine and sodium nitrite from Merck-India. All solvents were used as received and n-butyl nitrite was synthesized by reported method.[9b] ***Caution!*** *Perchlorates have to be handled with care and appropriate safety precautions!*

UV-vis spectra were recorded on a PerkinElmer LAMBDA 25 spectrophotometer. ^{1}H NMR spectra were measured on a Bruker FT 300 MHz spectrometer. Elemental analyses (C, H, N) were performed on a PerkinElmer 2400 series II analyzer and electrochemical measurements were recorded on a VersaStat II Princeton Applied Research potentiostat/galvanostat using a

platinum electrode under argon atmosphere. Tetraethylammonium perchlorate (TEAP) was used as a supporting electrolyte and potentials were referenced to the Ag/AgCl electrode without junction correction. Coulometric reduction was performed at a constant potential of –0.2 V *vs*. Ag/AgCl at 300 K in CH_3CN in the presence of NEt_4ClO_4 under argon. The emission data were collected on a PerkinElmer LS 55 fluorescence spectrometer. For all luminescence measurements excitation and emission slit widths of 3 nm was used. Quantum yields of complexes were determined at 25 °C in freeze–pump–thaw degassed solutions of acetonitrile. Anthracene in Ethanol and quinine bisulfate in 1 N H_2SO_4 are used as standard during quantum yield measurement for compounds **2** and $\mathbf{3}^+$ respectively.[17] The quantum yields were calculated using eqn (1)[18]:

$$\Phi_r = \Phi_{std} \frac{A_{std}}{A_r} \frac{I_r}{I_{std}} \frac{{\eta_r}^2}{{\eta_{std}}^2} \qquad (1)$$

where Φ_r and Φ_{std} are the quantum yields of unknown and standard samples (Φ_{std} = 0.546 for quinine bisulfate and Φ_{std} = 0. 270 for Anthracene), A_r and A_{std} are the solution absorbances at the excitation wavelength (λ_{ex}), I_r and I_{std} are the integrated emission intensities, and η_r and η_{std} are the refractive indices of the solvents. Time-correlated single-photoncounting (TCSPC) measurements were carried out for the luminescence decay of complexes in acetonitrile. For TCSPC measurement, the photoexcitation was made at 330 nm using a picosecond diode laser (IBH Nanoled-07) in an IBH Fluorocube apparatus. The fluorescence decay data were collected on a Hamamatsu MCP photomultiplier (R3809) and were analyzed by using IBH DAS6 software. Electron paramagnetic resonance (EPR) spectra were recorded for samples in standard quartz EPR tubes using a Varian E-109C spectrometer at the X-band. Magnetic susceptibilities were measured on a PAR- 155 vibrating-sample magnetometer fitted with a Walker Scientific magnet.

X-ray intensity data for compounds **2a** and $\mathbf{3a^+ClO_4^-}$ were measured at 293 (2) K on a Bruker AXS SMART APEX CCD diffractometer Mo Kα (λ = 0.71073 Å). Metal atoms were located by direct methods, and the rest of the non-hydrogen atoms emerged from successive Fourier synthesis. The structures were refined by full-matrix least-squares procedures on F^2. The hydrogen atoms were included in calculated positions and treated as riding atoms using

SHELXL default parameters. Calculations were performed using the SHELXTL V 6.14 program package.[19] Thermal ellipsoids were drawn at the 30% probability level. Molecular structure plots were drawn using the Oak Ridge thermal ellipsoid plot ORTEP.[20] Hydrogen atoms were kept fixed using the riding model during refinement for both **2** and $\mathbf{3a^{+}ClO_4^{-}}$.Crystallographic data and refinements for both of the complexes are presented in ESI (Table S9†). The ORTEP plots are presented in ESI (Fig. S12 and S13†)

In the case of complex $\mathbf{3a^{+}}$, the counter ClO_4^{-} anion was found to be disordered. After complete convergence of all of the non-hydrogen atoms of the complex cation, two crystallographically different perchlorate anions were located, each having half occupancy, from the difference Fourier map. The Cl atoms were disposed on the special positions in *C*2/c space group *viz*. Cl1 (0.50000 0.55490 0.25000) lied on crystallographic two-fold axes and Cl2 (0.50000 0.00000 0.50000) situated at crystallographic inversion centers and both were refined anisotropically. The peak height of chlorine atoms were ~12 e $Å^{-3}$, and significant peaks attached to the Cl2 atom with peak heights ranging from 2.35 to 2.48 e $Å^{-3}$ corresponded to disordered oxygen atoms. The O4 and O5 atoms comprise full occupancy and are bonded to Cl1 and Cl2 respectively. While the O3 and O6 atoms are found to be disordered over two sites and these two are split into 'O3A and O3B' and 'O6A and O6B' respectively by applying PART instruction. The relative occupancy factor for these disordered oxygen atoms are found to be about 65% and 35% for O3A and O3B atoms and 45% and 55% for O6A and O6B respectively. Inclusion of all of these oxygen atoms following the anisotropically refinement improved significantly the refinement parameters (R, wR_2, and goodness of fit) implying the right assignment of anion disorder.

Computational Study

The molecular geometry of the singlet ground state (S_0) and the first excited triplet state (T_1) of the synthesized complexes **2a** and $\mathbf{3a^{+}ClO_4^{-}}$ have been calculated by DFT method using the (R)B3LYP[21] hybrid functional approach incorporated in GAUSSIAN 09 program package.[22] The geometries of the complexes were fully optimized in gas phase without imposing any symmetry constraints. The nature of all the stationary points was checked by computing vibrational frequencies, and all the species were found to be true potential energy minima, as no imaginary frequency were obtained (NImag = 0). The single crystal X-ray coordinates have been used as

the initial input in all calculations for **2a** and **3a**$^{+}$**ClO**$_4^{-}$. The calculated S_0 structures nicely correspond to the geometrical parameters obtained experimentally by X-ray diffractometry. On the basis of the optimized ground and excited state geometries, the absorption and emission spectra properties in acetonitrile (CH_3CN) media were calculated by the time-dependent density functional theory (TD-DFT)[23] approach associated with the conductor-like polarizable continuum model (CPCM).[24] We computed the lowest 80 singlet–singlet transitions and 80 singlet–triplet transitions in absorption and emission processes respectively and the results of the TD calculations were qualitatively similar to the observed spectra. The TD-DFT approach is now well-known as a rigorous formalism for the treatment of electronic excitation energies within the DFT framework for calculating spectral properties of many transition metal complexes.[25] Hence TD-DFT had been shown to provide a reasonable spectral feature for the compounds under investigation. Moreover, to get an insight about the ground state geometry, electronic structure and nature of FMOs of **3**, it was optimized by assuming an S = ½ spin state at (U)B3LYP level.

The cobalt atom was described by a double-ζ basis set with the effective core potential of Hay and Wadt (LANL2DZ)[26] and the 6-31G basis set[27] was used for the other elements present in the complexes to optimize both the ground state and the lowest lying triplet excited state geometries. The calculated electronic density plots for frontier molecular orbitals were prepared by using the GaussView 5.0 software. GaussSum program, version 2.2[28] was used to calculate the molecular orbital contributions from groups or atoms.

Synthesis of the ligands

The ligands **1a** and **1b** were synthesized by reported method[9b] but with certain modifications, the details of which are reported below.

2-(Pyridylazo)benzaldoxime, HL^{Ph}, (1a). To an aqueous ethanolic (3:1) solution of 2.50 g (0.023 mol) of 2-hydrazinopyridine was added dropwise 2.43 g (0.022 mol) of benzaldehyde. The contents were allowed to stir for 2 h, and a white precipitate of the hydrazone, separated out. It was collected, washed with aqueous ethanol and then dried *in vacuo* over fused $CaCl_2$. Yield: 3.80 g (85%).

To a suspension of 3.80 g (0.019 mol) the hydrazone in 25 mL of dry ethanol was added 1.90 g (0.019 mol) of freshly prepared n-$BuNO_2$. To this mixture a solution of sodium ethoxide (prepared by refluxing 0.85 g of metallic sodium in 25 mL of dry ethanol) was added and the

mass was allowed to reflux for 3 hours when an intensely red coloured solution was obtained. It was then cooled and filtered into an ice-cold solution of sodium hydroxide (prepared by dissolving 1.0 g of NaOH in 100 mL of water). After 12 h, the solution was extracted with diethyl ether. The aqueous layer was separated from the mixture, cooled to 0 °C, and finally acidified with a 1N ice-cold solution of sulfuric acid to neutral pH. The contents were then extracted with dichloromethane and the organic extract was evaporated to isolate the ligand, **1a**. Yield: 2.80 g (68%). Elem. Anal. Calcd. (%) for **1a**, $C_{12}H_{10}N_4O$: C, 63.72; H, 4.42; N, 24.77. Found: C, 63.65; H, 4.38; N, 24.68. Mp: 103-105 °C. Elem. Anal. Calcd. (%) for **1b**, $C_{13}H_{12}N_4O$: C, 65.00; H, 5.00; N, 23.33. Found: C, 64.91; H, 5.05; N, 23.26. Mp: 100-102 °C.

Synthesis of the complexes

2a and **$3a^+ClO_4^-$.** To a methanolic solution of HL (0.061 g, 0.27 mmol) was added a methanolic solution of $Co(ClO_4)_2.6H_2O$ (0.05g, 0.13 mmol) and the dark coloured solution so formed was allowed to stir for 3 h. The deposited dark coloured precipitate was filtered off, washed several times with 1:1 aqueous ethanol and dried *in vacuo* over fused $CaCl_2$. The solid was recrystallized with dichloromethane-hexane layer when dark brown solid was precipitated out within two days and the solution remained violet. The violet solution was decanted off; the precipitate of **$3a^+ClO_4^-$** washed with hexane and dried *in vacuo*. Yield: 0.072 g (61%). Elem. Anal. Calcd. (%) for $C_{24}H_{18}N_8O_6ClCo$: C, 47.35; H, 2.98; N, 18.40. Found: C, 47.28; H, 2.95; N, 18.38. The violet solution was then evaporated to dryness to obtain the dark violet solid **2a**. Yield: 0.041 g (29%). Elem. Anal. Calcd. (%) for $C_{36}H_{27}N_{12}O_3Co$: C, 58.86; H, 3.70: N, 22.88. Found C, 58.46; H, 3.79: N, 22.58.

The complexes **2b** and **$3b^+ClO_4^-$** was prepared similarly. Elem. Anal. Calcd. (%) for $C_{26}H_{22}N_8O_6ClCo$: C, 49.03; H, 3.48; N, 17.59. Found for **$3b^+ClO_4^-$**: C, 49.12; H, 3.44; N, 17.54. Elem. Anal. Calcd. (%) for $C_{39}H_{33}N_{12}O_3Co$: C, 60.31; H, 4.28; N, 21.64. Found for **2b**: C, 60.81; H, 4.35; N, 21.45.

3a (*Electrochemical Method*). The complex **$3a^+ClO_4^-$** (0.06 g, 0.1 mmol) was dissolved in 25 ml of acetonitrile and to it tetraethyl ammonium perchlorate was added as supporting electrolyte. The brown mixture was stirred at room temperature for 0.25 h and the subject to exhaustive coulometric reduction at –0.2 V *vs*. SCE under nitrogen. The reduction was stopped when the coulomb count corresponded to one electron reduction and the solution turned pinkish brown.

The solvent was at first evaporated *in vacuo*, extracted with benzene and filtered. The filtrate was quickly evaporated *in vacuo* to obtain **3a** as dark solid in pure form. Yield: 0.043 g (86%). Elem. Anal. Calcd. (%) for $C_{24}H_{18}N_8O_2Co$: C, 56.41; H, 3.45; N, 21.92. Found: C, 56.51; H, 3.49; N, 22.08. The complex **3b** was synthesized similarly in 88% yield. Elem. Anal. Calcd. (%) for $C_{26}H_{22}N_8O_2Co$: C, 58.02; H, 4.10; N, 20.69. Found: C, 58.17; H, 4.07; N, 20.80.

3a (*Chemical Method*). To an acetonitrile solution of $\mathbf{3a^+ClO_4^-}$ (0.06 g, 0.1 mmol), a drop of hydrazine hydrate was added and the contents stirred when the solution turned pinkish brown. It was then quickly evaporated, washed with water and dried *in vacuo* over fused $CaCl_2$ to obtain **3a**. Yield: 0.037 (74%). The complex **3b** was synthesized chemically by similar procedure.

Acknowledgements

We thank the Department of Science and Technology, New Delhi, for financial assistance (Grant SR/S1/IC-75/2010). We are also thankful to Department of Science and Technology, New Delhi, India for the data collection on the CCD facility setup (Jadavpur University). We also acknowledge CAS, Department of Chemistry, Jadavpur University and the DST-PURSE program for other facilities. Thanks to Dr. Ayan Datta of IACS, Kolkata for computational assistance. Special thanks to Dr. Deepak Chopra of IISER, Bhopal for his suggestion in crystal structure refinement. Mr. S. Pramanik and Mr. T. Ghorui thanks the UGC, New Delhi and Ms. S. Roy thanks DST for the research fellowship.

Supporting Information Available

† Electronic supplementary information (ESI) available: NMR , absorption, emission spectra and photoluminescence decay of ligand, Tables and Figures for TD-DFT of complexes, crystallographic data and structure refinement parameters and ORTEP plot of **2a** and $\mathbf{3a^+}$, coordinates of optimized geometries of complexes. CCDC 964213–964214. For ESI and crystallographic data in CIF or other electronic format see DOI:

References

1 (*a*) G. N. Schrauzer and R. J. Windgassen, *J. Am. Chem. Soc.*, 1966, **88**, 3738; (*b*) G. N. Schrauzer and J. Kohnle, *Chem. Ber.*, 1964, **97**, 3056.
2 (*a*) B. H. Solis, Y. Yu and S. Hammes-Schiffer, *Inorg. Chem.*, 2013, **52**, 6994; (*b*) F. Lakadamyali, M. Kato, N. M. Muresan and E. Reisner, *Angew. Chem., Int. Ed.*, 2012, **51**, 9381;

(*c*) C. C. L. McCrory, C. Uyeda and J. C. Peters, *J. Am. Chem. Soc.*, 2012, **134**, 3164; (*d*) V. Artero, M. Chavarot-Kerlidou and M. Fontecave, *Angew. Chem., Int. Ed.*, 2011, **50**, 7238; (*e*) B. Probst, M. Guttentag, A. Rodenberg, P. Hamm and R. Alberto, *Inorg. Chem.*, 2011, **50**, 3404; (*f*) J. L. Dempsey, B. S. Brunschwig, J. R.Winkler and H. B. Gray, *Acc. Chem. Res.*, 2009, **42**, 1995.

3 (*a*) J. A. Kim, S. Kim, J. Lee, J.-O. Baeg and J. Kim, *Inorg. Chem.*, 2012, **51**, 8057; (*b*) S. Abdel-Azeim, X. Li, L. W. Chung and K. Morokuma, *J. Comput Chem.*, 2011, **32**, 3154.

4 (*a*) C. C. L. McCrory, C. Uyeda and J. C. Peters, *J. Am. Chem. Soc.*, 2012, **134**, 3164; (*b*) A. Bhattacharjee, M. Chavarot-Kerlidou, E. S. Andreiadis, M. Fontecave, M. J. Field and V. Artero, *Inorg. Chem.*, 2012, **51**, 7087; (*c*) P. Zhang, P.-A. Jacques, M. Chavarot-Kerlidou, M. Wang, L. Sun, M. Fontecave and V. Artero, *Inorg. Chem.*, 2012, **51**, 2115; (*d*) M. Wang, Y. Na, M. Gorlov and L. C. Sun, *Dalton Trans.*, 2009, 6458; (*e*) X. Hu, B. M. Cossairt, B. S. Brunschwig, N. S. Lewis and J. C. Peters, *Chem. Commun.*, 2005, 4723.

5 (*a*) A. Krawicz, J. Yang, E. Anzenberg, J. Yano, I. D. Sharp and G. F. Moore, *J. Am. Chem. Soc.*, 2013, **135**, 11861; (*b*) B. H.Solis, Y. Yu and S. Hammes-Schiffer, *Inorg. Chem.*, 2013, **52**, 6994; (*c*) J. Niklas, K. L. Mardis, R. R. Rakhimov, K. L. Mulfort, D. M. Tiede and O. G. Poluektov, *J. Phys. Chem. B*, 2012, **116**, 2943; (*d*) B. H. Solis and S. Hammes-Schiffer, *J. Am. Chem. Soc.*, 2011, **133**, 19036; (*e*) B. H. Solis and S. Hammes-Schiffer, *Inorg. Chem.*, 2011, **50**, 11252; (*f*) T. M. McCormick, Z. Han, D. J. Weinberg, W. W. Brennessel, P. L. Holland and R. Eisenberg, *Inorg. Chem.*, 2011, **50**, 10660; (*g*) B. Probst, M. Guttentag, A. Rodenberg, P. Hamm and R. Alberto, *Inorg. Chem.*, 2011, **50**, 3404; (*h*) T. M. McCormick, B. D. Calitree, A. Orchard, N. D. Kraut, F. V. Bright, M. R. Detty and R. Eisenberg, *J. Am. Chem. Soc.*, 2010, **132**, 15480; (*i*) K. L. Mulfort and D. M. Tiede, *J. Phys. Chem. B*, 2010, **114**, 14572; (*j*) T. Lazarides, T. McCormick, P. Du, G. Luo, B. Lindley and R. Eisenberg, *J. Am. Chem. Soc.*, 2009, **131**, 9192.

6 (*a*) S. Joy, T. Krämer, N. D. Paul, P. Banerjee, J. E. McGrady and S. Goswami, *Inorg. Chem.*, 2011, **50**, 9993; (*b*) N. Paul, S. Samanta and S. Goswami, *Inorg. Chem.*, 2010, **49**, 2649; (*c*) P. Banerjee, S. Sproules, T. Weyhermüller, S. D. George and K. Wieghardt, *Inorg. Chem.*, 2009, **48**, 5829; (*d*) B. Sarkar, S. Patra, J. Fiedler, R. B. Sunoj, D. Janardanan, G. K. Lahiri and W. Kaim, *J. Am. Chem. Soc.*, 2008, **130**, 3532; (*e*) S. Samanta, P. Singh, J. Fiedler, S. Záliš, W. Kaim and S. Goswami, *Inorg. Chem.*, 2008, **47**, 1625; (*f*) S. Blanchard, N. Neese, N. E. Bothe, E. Bill, T. Weyhermüller and K. Wieghardt, *Inorg. Chem.*, 2005, **44**, 3636; (*g*) M. Shivakumar, K. Pramanik, I. Bhattacharyya and A. Chakravorty, *Inorg. Chem.*, 2000, **39**, 4332; (*h*) K. Pramanik, M. Shivakumar, P. Ghosh and A. Chakravorty, *Inorg. Chem.*, 2000, **39**, 195; (*i*) N. Doslik, T. Sixt and W. Kaim, *Angew. Chem., Int. Ed.*, 1998, **37**, 2403; (*j*) M. Shivakumar, K. Pramanik, P. Ghosh and A. Chakravorty, *Inorg. Chem.*, 1998, **37**, 5968.

7 (*a*) N. D. Paul, U. Rana, S. Goswami, T. K. Mondal and S. Goswami, *J. Am. Chem. Soc.*, 2012, **134**, 6520; (*b*) N. C. Tomson, M. R. Crimmin, T. Petrenko, L. E. Rosebrugh, S. Sproules, W. C. Boyd, R. G. Bergman, S. DeBeer, F. D. Toste and K. Wieghardt, *J. Am. Chem. Soc.*, 2011, **133**, 18785; (*c*) W. Kaim, *Inorg. Chem.*, 2011, **50**, 9752; (*d*) A. K. Das, B. Sarkar, J. Fiedler, S. Zális, I. Hartenbach, S. Strobel, G. K. Lahiri and W. Kaim, *J. Am. Chem. Soc.*, 2009, **131**, 8895; (*e*) C. C. Lu, E. Bill, T. Weyhermüller, E. Bothe and K. Wieghardt, *J. Am. Chem. Soc.*, 2008, **130**, 3181; (*f*) K. Pramanik, U. Das, B. Adhikari, D. Chopra and H. Stoeckli-Evans, *Inorg. Chem.*, 2008, **47**, 429.

8 (*a*) C. H. Langford and A. Y. S. Malkhasian, *J. Am. Chem. Soc.*, 1987, **109**, 2682; (*b*) K. Zahir, W. Böttcher and A. Haim, *Inorg. Chem.*, 1985, **24**, 1966; (*c*) B. R. Hollebone, C. H. Langford and A. Y. S. Malkhasian, *Can. J. Chem.*, 1985, **63**, 1918; (*d*) D. Sandrini, M. T. Gandolfi, M.

Maestri, F. Bolletta and V. Balzani, *Inorg. Chem.*, 1984, **23**, 3017; (*e*) V. H. Houlding and V. M. Miskowski, *Inorg. Chem.*, 1984, **23**, 4671.
9 (*a*) C. K. Pal and S. Ganguly, *J. Ind. Chem. Soc.*, 2002, **79**, 271; (*b*) S. Ganguly, S. Karmakar, C. K. Pal and A. Chakravorty, *Inorg. Chem.*, 1999, **38**, 5984.
10 (*a*) S. Ganguly, V. Manivannan and A. Chakravorty, *J. Chem. Soc., Dalton Trans.*, 1998, 461; (*b*) S. Karmakar, S. B. Chowdhury, S. Ganguly, and A. Chakravorty, *J. Chem. Soc., Dalton Trans.*, 1997, 585; (*c*) V. Manivannan, B. K. Dirghangi, C. K. Pal and A. Chakravorty, *Inorg. Chem.*, 1997, **36**, 1526; (*d*) C. K. Pal, S. Chattopadhyay, C. Sinha and A. Chakravorty, *Inorg. Chem.*, 1994, **33**, 6140; (*e*) D. Bandyopadhyay, P. Bandyopadhyay, A. Chakravorty, F. A. Cotton and L. R. Falvello, *Inorg. Chem*, 1984, **23**, 1785; (*f*) P. Bandyopadhyay, D. Bandyopadhyay, A. Chakravorty, F. A. Cotton, L. R. Falvello and S. Han, *J. Am. Chem. Soc.*, 1983, **105**, 6327; (*g*) P. Bandyopadhyay, P. K. Mascharak, and A. Chakravorty, *J. Chem. Soc., Dalton Trans.*, 1982, 675; (*h*) P. K. Mascharak and A. Chakravorty, *J. Chem. Soc., Dalton Trans.*, 1980, 1698; (*i*) M. H. Dickmann and R. J. Deodens, *Inorg. Chem.*, 1980, **19**, 3112.
11 (*a*) V. Manivannan, S. Datta, P. Basu and A. Chakravorty, *Inorg. Chem*, 1993, **22**, 4807; (*b*) V. Manivannan, S. Chattopadhyay, P. Basu and A. Chakravorty, *Polyhedron*, 1993, **12**, 2725; (*c*) P. Basu, S. Pal and A. Chakravorty, *J. Chem. Soc., Dalton Trans.*, 1991, 3217; (*d*) S. Chattopadhyay, P. Basu, S. Pal and A. Chakravorty, *J. Chem. Soc., Dalton Trans.*, 1990, 3829; (*e*) S. Pal, R. N. Mukherjee, M. Thomas, L. R. Falvello and A. Chakravorty, *Inorg. Chem.*, 1986, **25**, 200.
12 (*a*) S. Ganguly, *J. Ind. Chem. Soc*., 2012, **89**, 107; (*b*) I. Bhattacharyya and S. Ganguly, *J. Ind. Chem. Soc*., 2010, **87**, 1299; (*c*) I. Bhattacharyya, S. Ganguly, B. K. Panda and A. Chakravorty, *J. Chem. Sci*., 2008, **120**, 87.
13 J. E. Huheey, E. A. Keiter and R. L. Keiter, *Inorganic Chemistry: Principles of structure and reactivity*, HarperCollins College Publishers, New York, 4th Edition, 2007.
14 (a) P. Mondal, A. Hens, S. Basak and K. K. Rajak, *Dalton Trans.*, 2013, **42**, 1536; (b) L. Szabó, K. Herman, N. E. Mircescu, A. Fălămaş, L. F. Leopold, N. Leopold, C. Buzumurgă and V. Chiş, *Spectrochim Acta A*, 2012, **93**, 266; (c) K. Pramanik and B. Adhikari, *Polyhedron*, 2010, **29**, 1015.
15 S. Ross, T. Weyhermüller, E. Bill, K. Wieghardt and P. Chaudhuri, *Inorg. Chem.*, 2001, **40**, 6656.
16 (*a*) A. Kochem, H. Kanso, B. Baptiste, H. Arora, C. Philouze, O. Jarjayes, H. Vezin, D. Luneau, M. Orio and F. Thomas, *Inorg. Chem.*, 2012, **51**, 10557; (*b*) G. M. Zats, H. Arora, R. Lavi, D. Yufit and L. Benisvy, *Dalton Trans.*, 2011, **40**, 10889; (*c*) E. Vinck, D. M. Murphy, I. A. Fallis, R. R. Strevens and S. V. Doorslaer, *Inorg. Chem.*, 2010, **49**, 2083; (*d*) A. S. Roy, N. Muresan, H. M. Tuononen, S. P. Rath and P. Ghosh, *Dalton Trans.*, 2008, 3438; (*e*) Y. Shimazaki, R. Kabe, S. Huth, F. Tani, Y. Naruta and O. Yamauchi, *Inorg. Chem.*, 2007, **46**, 6083; (*f*) E. Bill, E. Bothe, P. Chaudhuri, K. Chlopek, D. Herebian, S. Kokatam, K. Ray, T. Weyhermüller, F. Neese and K. Wieghardt, *Chem. Eur. J.*, 2005, **11**, 204; (*g*) L. Benisvy, E. Bill, A. J. Blake, D. Collison, E. S. Davies, C. D. Garner, C. I. Guindy, E. J. L. McInnes, G. McArdle, J. McMaster, C. Wilson and J. Wolowska, *Dalton Trans.*, 2004, 3647; (*h*) S. Kimura, E. Bill, E. Bothe, T. Weyhermüller and K. Wieghardt, *J. Am. Chem. Soc.*, 2001, **123**, 6025; (*i*) J. Müller, A. Kikuchi, E. Bill, T. Weyhermüller, P. Hildebrandt, L. Ould-Moussa and K. Wieghardt, *Inorg. Chim. Acta.*, 2000, **297**, 265; (*j*) C. N. Verani, S. Gallert, E. Bill, T. Weyhermüller, K. Wieghardt and P. Chaudhuri, *Chem. Commun.*, 1999, 1747; (*k*) S. Arzberger, J. Soper, O. P. Anderson, A. la Cour and M. Wicholas, *Inorg. Chem.*, 1999, **38**, 757; (*l*) A. Sokolowski, B. Adam, T.

Weyhermüller, A. Kikuchi, K. Hilden-brand, R. Schnepf, P. Hildebrandt, E. Bill and K. Wieghardt, *Inorg. Chem.*, 1997, **36**, 3702; (*m*) C. W. Lange, B. J. Conklin and C. G. Pierpont, *Inorg. Chem.*, 1994, **33**. 1276.
17 (*a*) S. R. Meech and D. Phillips, *J. Photochem.*, 1983, **23**, 193 and references therein; (*b*) W. R. Dawson and M. W. Windsor, *J. Phys. Chem.*, 1968, **72**, 3251 and references therein.
18 J. van Houten and R. J. Watts, *J. Am. Chem. Soc.*, 1976, **98**, 4853.
19 G. M. Sheldrick, *SHELXTL v. 6.14*, Bruker AXS Inc., Madison, WI, 2003.
20 C. K. Johnson, ORTEP Report ORNL-5138, Oak Ridge National Laboratory, Oak Ridge, TN, 976.
21 (*a*) A. D. Becke, *J. Chem. Phys.*, 1993, **98**, 5648; (*b*) C. Lee, W. Yang and R. G. Parr, *Phys. Rev. B*, 1988, **37**, 785.
22 Gaussian 09, Revision A.01, M. J. Frisch, G. W. Trucks, H. B. Schlegel, G. E. Scuseria, M. A. Robb, J. R. Cheeseman, G. Scalmani, V. Barone, B. Mennucci, G. A. Petersson, H. Nakatsuji, M. Caricato, X. Li, H. P. Hratchian, A. F. Izmaylov, J. Bloino, G. Zheng, J. L. Sonnenberg, M. Hada, M. Ehara, K. Toyota, R. Fukuda, J. Hasegawa, M. Ishida, T. Nakajima, Y. Honda, O. Kitao, H. Nakai, T. Vreven, J. A. Montgomery, Jr., J. E. Peralta, F. Ogliaro, M. Bearpark, J. J. Heyd, E. Brothers, K. N. Kudin, V. N. Staroverov, R. Kobayashi, J. Normand, K. Raghavachari, A. Rendell, J. C. Burant, S. S. Iyengar, J. Tomasi, M. Cossi, N. Rega, J. M. Millam, M. Klene, J. E. Knox, J. B. Cross, V. Bakken, C. Adamo, J. Jaramillo, R. Gomperts, R. E. Stratmann, O. Yazyev, A. J. Austin, R. Cammi, C. Pomelli, J. W. Ochterski, R. L. Martin, K. Morokuma, V. G. Zakrzewski, G. A. Voth, P. Salvador, J. J. Dannenberg, S. Dapprich, A. D. Daniels, O. Farkas, J. B. Foresman, J. V. Ortiz, J. Cioslowski and D. J. Fox, Gaussian, Inc., Wallingford CT, 2009.
23 (*a*) J. Autschbach, T. Ziegler, S. J. A. Gisbergen and E. J. Baerends, *J. Chem. Phys.*, 2002, **116**, 6930; (*b*) K. L. Bak, P. Jørgensen, T. Helgaker, K. Rund and H. J. A. Jenson, *J. Chem. Phys.*, 1993, **98**, 8873; (*c*) T. Helgaker and P. Jørgensen, *J. Chem. Phys.*, 1991, **95**, 2595; (*d*) E. K. U. Gross and W. Kohn, *Adv. Quantum Chem.*, 1990, **21**, 255.
24 (*a*) M. Cossi, N. Rega, G. Scalmani and V. Barone, *J. Comput. Chem.*, 2003, **24**, 669; (*b*) M. Cossi and V. Barone, *J. Chem. Phys.*, 2001, **115**, 4708; (*c*) V. Barone and M. Cossi, *J. Phys. Chem. A*, 1998, **102**, 1995.
25 (*a*) T. Liu, H. X. Zhang and B. H. Xia, *J. Phys. Chem. A*, 2007, **111**, 8724; (*b*) A. Albertino, C. Garino, S. Ghiani, R. Gobetto, C. Nervi, L. Salassa, E. Rosenverg, A. Sharmin, G. Viscardi, R. Buscaino, G. Cross and M. Milanesio, *J. Organomet. Chem.*, 2007, **692**, 1377; (*c*) X. Zhou, H. X. Zhang, Q. J. Pan, B. H. Xia and A. C. Tang, *J. Phys. Chem. A*, 2005, **109**, 8809; (*d*) X. Zhou, A. M. Ren and J. K. Feng, *J. Organomet. Chem.*, 2005, **690**, 338.
26 (*a*) P. J. Hay and W. R. Wadt, *J. Chem. Phys.*, 1985, **82**, 299; (*b*)P. J. Hay and W. R. Wadt, *J. Chem. Phys.*, 1985, **82**, 270.
27 (*a*) M. S. Gordon, J. S. Binkley, J. A. Pople, W. J. Pietro and W. J. Hehre, *J. Am. Chem. Soc.*, 1982, **104**, 2797; (*b*) J. S. Binkley, J. A. Pople and W. J. Hehre, *J. Am. Chem. Soc.*, 1980, **102**, 939.
28 N. M. O'Boyle, A. L. Tenderholt and K. M. Langner. *J. Comp. Chem.*, 2008, **29**, 839.

Graphical Abstract for the contents

Molecular and Electronic Structure of Nonradical Homoleptic Pyridyl-azo-oxime Complexes of Cobalt(III) and the Azo-oxime Anion Radical Congener: An Experimental and Theoretical Investigation

Shuvam Pramanik, Sima Roy, Tapas Ghorui, Sanjib Ganguly* and Kausikisankar Pramanik*

Synthesis and optoelectronic characterization of a pair of homoleptic cobalt(III) complexes incorporating pyridyl-azo-oxime with subsequent isolation of Co(III)-bound stable azo-oxime Anion radical — an experimental and theoretical investigation.